

4
5 The authors used the CESM model with a source-tagging method to quantify the
6 source attributions for BC direct radiative forcing (DRF) and concentration as well as
7 polluted events. They found that in addition to regional emissions within China,
8 emissions outside China also contribute to a large portion of BC DRF over China.
9 This study could improve the understanding on BC pollution in China and provide
10 implications for policy makers. Before this manuscript can be considered for
11 publication, I have a few comments that need to be addressed by the authors.
12

13 1. One critical factor influencing BC direct radiative effect is its optical properties
14 (absorption and extinction cross section, asymmetry factor, and single scattering
15 albedo). Recent studies (e.g., He et al. 2015, 2016b) showed that BC optical
16 properties vary significantly (by up to more than a factor of two) due to different
17 coating structures and aging stages during BC aging process, which further affects
18 direct radiative effect. (1) Could the authors add some discussions on this aspect with
19 reference to these recent studies, for example, potential uncertainty in their results
20 caused by this factor? (2) Could this variation in BC optical properties due to coating
21 structures contribute to the model biases in BC AAOD simulations as discussed in the
22 first paragraph of Section 3.2? (3) It would be helpful if the authors could add more
23 details on how the MAM3 model computes BC optical properties. For example, does
24 it assume a core-shell structure for internally mixed BC?

25 References:

26 He, C., et al. : Variation of the radiative properties during black carbon aging:
27 theoretical and experimental intercomparison, *Atmos. Chem. Phys.*, 15,
28 11967-11980, doi:10.5194/acp-15-11967-2015, 2015.

29 He, C., et al. : Intercomparison of the GOS approach, superposition T-matrix method,
30 and laboratory measurements for black carbon optical properties during aging, *J.*
31 *Quant. Spectrosc. Radiat. Transf.*, 184, 287–296, doi:10.1016/j.jqsrt.2016.08.004,
32 2016b.

33
34 Response:

35 (1) Thanks for the suggestion. We have added discussions of the influence of
36 aging processes on BC optical properties to the Conclusions and Discussions
37 section, along with the references provided by the referee, as “BC aging in the
38 atmosphere is important for BC concentration and its optical properties, which
39 transforms BC from hydrophobic aggregates to hydrophilic particles coated with
40 soluble materials. He et al. (2015, 2016a) found that BC optical properties varied by a
41 factor of two or more due to different coating structures during BC aging process
42 based on their theoretical and experimental intercomparison. Oshima et al. (2009)
43 and He et al. (2016b) pointed out that the use of various microphysical BC aging
44 schemes could significantly improve simulations of BC concentrations compared to

45 the simplified aging parameterizations. Liu et al. (2012) also reported that the wet
46 removal rate of BC simulated in standard CAM5 is 60% higher than AeroCom
47 multi-model mean due to the rapid or instantaneous aging of BC. H. Wang et al.
48 (2013) showed that the explicit treatment of BC aging process with slow aging
49 assumptions in CAM5 could significantly increase BC lifetime and the efficiency of BC
50 long-range transport. In the three-mode aerosol module (MAM3) of CAM5 used in this
51 study, the aging process of BC is neglected by assuming the immediate internal
52 mixing of BC with other aerosol species in the same mode. This assumption could
53 lead to an overestimation of wet removal of BC and, therefore, an underestimation of
54 BC concentrations, absorption optical depth (Fig. 3) and direct radiative forcing. In
55 addition, the internally-mixed optical treatment in CAM5 could also cause bias in BC
56 absorption calculation. However, H. Wang et al. (2014) examined source-receptor
57 relationships for BC under the different BC aging assumptions and found that the
58 quantitative source attributions varied slightly while the qualitative source-receptor
59 relationships still hold. Therefore, although the magnitude of simulated BC and its
60 optical properties could be underestimated due to the instantaneous aging of BC and
61 uncertainty in coating structures, we expect that the aging treatment in MAM3 of
62 CAM5 should not influence the qualitative source attributions examined in this study.”

63 (2) We agree that uncertainties in BC optical properties due to coating structures
64 and/or aging could contribute to model biases in simulated BC concentrations and
65 AAOD. We have added this statement in the discussion section. Please see the
66 revisions above.

67 (3) In the MAM3 aerosol module of CAM5 used in this study, the aging process of
68 BC is neglected by assuming an instantaneous mixing of BC with other aerosol
69 species in the same accumulation mode, which has been added in the discussion
70 section. We also add a more detailed description of the calculation of aerosol optical
71 properties in the Methods section, as “Aerosol optical properties for each mode are
72 parameterized according to Ghan and Zaveri (2007). Refractive indices for aerosols
73 are taken from the OPAC (optical properties for aerosols and clouds) software
74 package (Koepke and Schult, 1998), but for BC at solar wavelengths the values are
75 updated from Bond and Bergstrom (2006).”

76
77 2. For BC emissions, a number of global and regional emission inventories have been
78 developed, which showed large uncertainties and differences among each other
79 (e.g., Fig. 4 in Wang et al., 2014). It would be helpful if the authors could discuss the
80 uncertainty associated with the emission inventory used in this study and how this
81 inventory compares with previous ones for both inside and outside China, since the
82 authors pointed out that emissions outside China also contribute a lot to BC DRF in
83 China.

84
85 Reference:

86 Wang, R., et al. : Trend in Global Black Carbon Emissions from 1960 to 2007,
87 Environ. Sci. Technol., 48, 6780–6787, doi: 10.1021/es5021422, 2014.

88

89 Response:

90 Uncertainty in China BC emissions has been estimated as –43% to 93% by Lu et
91 al. (2011), –50% to 164% by Qin and Xie (2012), ±176% by Kurokawa et al. (2013),
92 and –28 to 126% by Zhao et al. (2013). The BC emissions estimates used here for
93 China in 2010 are 40% higher than those of Zhao et al. (2013) and Lu et al. (2011)
94 and 30% higher than Klimont et al. (2016), in large part due to a higher estimate of
95 BC emissions from coal coke production. Emissions from coke production are
96 particularly uncertain given that “there are no measurements for PM_{2.5} and BC
97 emissions” (Huo et al. 2012) available to guide inventory estimates. Total rest of the
98 world emissions other than China, which appear to be a major contributor to burdens
99 over western regions, are within 1% of those from Klimont et al. (2016). We have
100 added these discussions in Conclusions and discussions section.

101 We have added Table S1 to compare the anthropogenic emissions used in this
102 study with emissions from some previous studies. The anthropogenic emissions of
103 BC in China in 2010–2014 are larger than those used in the previous studies for
104 earlier years, partly as a result of a higher estimate of BC emissions from coal coking
105 production. The higher emissions likely lead to higher concentrations and direct
106 radiative forcing, and source contributions of BC in China, compared to the values
107 reported in these studies. We have added these descriptions in the Methods section.

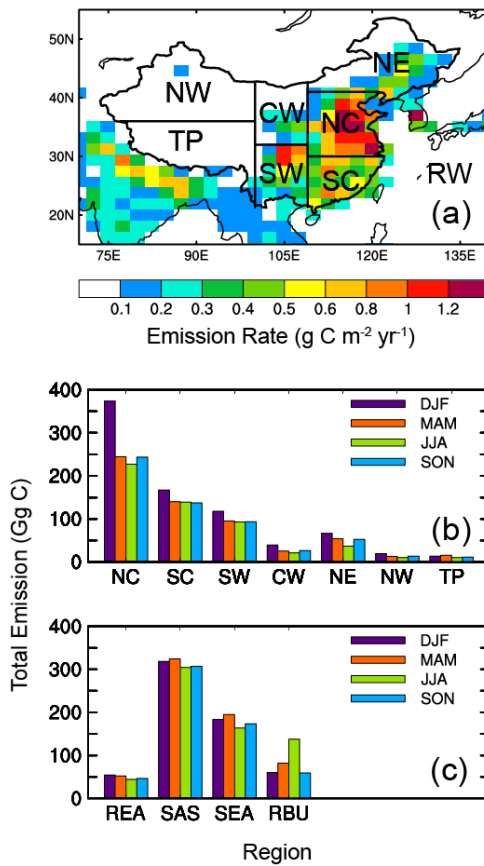
108 We also revised Fig. 1 to include BC emissions from outside China. Emissions at
109 regional scale are summarized here instead of Country level because the model
110 revolution is a bit course to characterize emissions by countries. Total BC emissions
111 from neighboring regions including rest of East Asia (REA, with China excluded),
112 South Asia (SAS), Southeast Asia (SEA), and Russia/Belarusia/Ukraine (RBU) are
113 shown in Figure 1c. These source regions outside China are consistent with source
114 regions defined in the second phase of Hemispheric Transport of Air Pollution
115 (HTAP2). South Asia and Southeast Asia have relatively high emissions. They may
116 dominate the contribution to concentrations and direct radiative forcing of BC in
117 China, especially southern and western China, from foreign sources through
118 long-range transport. We have also added these in the Methods section. We did not
119 compare the emissions outside China with other studies, which is beyond the scope
120 of this study. However, the comparison of CEDS emissions with other emission
121 inventories can be found in Hoesly et al. (2017), which includes detailed information
122 of the CEDS emissions and will be submit very soon.

123
124
125
126
127
128
129
130
131

132 **Table S1.** Comparison of CEDS annual mean anthropogenic BC emissions in China
 133 with those used in other studies
 134

	Year	Anthropogenic emission in China (Gg/yr)
CEDS		
(Hoesly et al., 2016; this study)	2010–2014	2467
MIX (Li et al., 2017)	2010	1765
HTAP V2.2 (Janssens- Maenhout et al., 2015)	2010	1741
Lu et al. (2011)	2010	1751
Qin and Xie (2012)	2009	1764
Wang et al. (2012)	2007	1879
INTEX-B (Zhang et al., 2009)	2006	1811

135



136

137

138 **Figure 1.** (a) Spatial distribution of annual mean total emissions (anthropogenic plus
139 biomass burning, units: $\text{g C m}^{-2} \text{ yr}^{-1}$) of black carbon (BC) averaged over 2010–2014.
140 The geographical BC source regions are selected as North China (NC, 109°E–east
141 boundary, 30°–41°N), South China (SC, 109°E–east boundary, south boundary–
142 30°N), Southwest China (SW, 100°–109°N, south boundary–32°N), Central-West
143 China (CW, 100°–109°N, 32°N–north boundary), Northeast China (NE, 109°E–east
144 boundary, 41°N–north boundary), Northwest China (NW, west boundary–100°E,
145 36°N–north boundary), and Tibetan Plateau (TP, west boundary–100°E, south
146 boundary–36°N) in China and regions outside of China (RW, rest of the world). (b)
147 Seasonal mean total emissions (units: Gg C , $\text{Gg} = 10^9\text{g}$) of BC from the seven BC
148 source regions in China and (c) emissions from rest of East Asia (REA, with China
149 excluded), South Asia (SAS), Southeast Asia (SEA), and Russia/Belarusia/Ukraine
150 (RBU).

151

152

153 3. Another important factor affecting BC simulations is aging process, which directly
154 alters BC wet scavenging and lifetime. As pointed out by some recent studies (e.g.,
155 Oshima et al., 2009; He et al., 2016a), applying microphysical BC aging schemes
156 could significantly improve simulations of BC concentrations compared with simplified
157 aging parameterizations. (1) Could the authors briefly describe how BC aging is
158 treated/computed in their model? (2) It would be helpful if the authors could briefly
159 discuss the BC aging effect on their results with reference to these recent studies. (3)
160 The authors mentioned in Lines 255–256 that model biases in BC concentration over
161 China is likely due to inaccurate emissions and wet scavenging. Could this bias also
162 be caused by model uncertainty related to BC aging? Some discussions would be
163 useful.

164

165 reference:

166

167 He, C., Li, Q., Liou, K.-N., Qi, L., Tao, S., and Schwarz, J. P.: Microphysics-based
168 black carbon aging in a global CTM: constraints from HIPPO observations and
169 implications for global black carbon budget, *Atmos. Chem. Phys.*, 16, 3077–3098,
170 doi:10.5194/acp-16-3077-2016, 2016a.

171

172 Oshima, N., et al. : Aging of black carbon in outflow from anthropogenic sources
173 using a mixing state resolved model: Model development and evaluation, *J. Geophys.*
174 *Res.*, 114, D06210, doi:10.1029/2008JD010680, 2009.

175

176 **Response:**

177 (1) Thanks for the suggestion. We had now added more description of the BC
178 aging treatment and related discussions to the paper. Please see the response to
179 comment #1 above.

180 (2) Following the referee's suggestion, we had now added more discussions in
181 this regard. Please see the response to comment #1 above.

182 (3) Yes, the overestimation of wet scavenging is partly caused by the assumption
183 of instantaneous aging of BC in the model. We have added the message to the
184 manuscript, as "Larger wet removal rate and shorter lifetime of aerosols along with
185 the instantaneous aging of BC in the MAM3 can also lead to the lower concentrations
186 of BC (e.g., Wang et al., 2011; Liu et al., 2012; H. Wang et al., 2013; Kristiansen et
187 al., 2016)." and in discussion section as "This assumption could lead to an
188 overestimation of wet removal of BC and, therefore, an underestimation of BC
189 concentrations, absorption optical depth (Fig. 3) and direct radiative forcing."
190

191 4. The authors derived BC AAOD from AERONET observations by using the method
192 in Bond et al. (2013). However, a recent study by Schuster et al. (2016) pointed out
193 some weaknesses and problems related to the Bond et al. (2013) method. Could the
194 author briefly discuss this issue? How would this affect the results in this study?
195

196 Reference:

197 Schuster, G. L., et al. : Remote sensing of soot carbon – Part 2: Understanding the
198 absorption Ångström exponent, *Atmos. Chem. Phys.*, 16, 1587–1602,
199 doi:10.5194/acp-16-1587-2016, 2016.
200

201 Response:

202 We have included a discussion of this caveat associated with the BC AAOD
203 comparison, as "Note that, the observed AAOD of BC is derived from AERONET
204 measurements using the absorption Ångström exponent. A recent study (Schuster et
205 al., 2016) reported that absorption Ångström exponent is not a robust parameter for
206 separating out carbonaceous absorption in the AERONET database, which could
207 cause biases in the AAOD estimates."
208
209
210

211 References:

212 He, C., Liou, K.-N., Takano, Y., Zhang, R., Levy Zamora, M., Yang, P., Li, Q., and
213 Leung, L. R.: Variation of the radiative properties during black carbon aging:
214 theoretical and experimental intercomparison, *Atmos. Chem. Phys.*, 15,
215 11967-11980, doi:10.5194/acp-15-11967-2015, 2015.
216

217 He, C., Takano, Y., Liou, K.-N., Yang, P., Li, Q., and Mackowski, D. W.:
218 Intercomparison of the GOS approach, superposition T- matrix method, and
219 laboratory measurements for black carbon optical properties during aging, *J.*
220 *Quant. Spectrosc. Ra.*, 184, 287–296, doi:10.1016/j.jqsrt.2016.08.004, 2016a.
221

222 Kristiansen, N. I., Stohl, A., Olivíe, D. J. L., Croft, B., Søvde, O. A., Klein, H.,
223 Christoudias, T., Kunkel, D., Leadbetter, S. J., Lee, Y. H., Zhang, K., Tsigaridis,

224 K., Bergman, T., Evangeliou, N., Wang, H., Ma, P.-L., Easter, R. C., Rasch, P. J.,
225 Liu, X., Pitari, G., Di Genova, G., Zhao, S. Y., Balkanski, Y., Bauer, S. E.,
226 Faluvegi, G. S., Kokkola, H., Martin, R. V., Pierce, J. R., Schulz, M., Shindell, D.,
227 Tost, H., and Zhang, H.: Evaluation of observed and modelled aerosol lifetimes
228 using radioactive tracers of opportunity and an ensemble of 19 global models,
229 *Atmos. Chem. Phys.*, 16, 3525-3561, doi:10.5194/acp-16-3525-2016, 2016.
230
231 Liu, X., et al. (2012), Toward a minimal representation of aerosols in climate models:
232 Description and evaluation in the Community Atmosphere Model CAM5, *Geosci.
233 Model Dev.*, 5, 709–739, doi:10.5194/gmd-5-709-2012.
234
235 Liu, X., Ma, P.-L., Wang, H., Tilmes, S., Singh, B., Easter, R. C., Ghan, S. J., and
236 Rasch, P. J.: Description and evaluation of a new four-mode version of the Modal
237 Aerosol Module (MAM4) within version 5.3 of the Community Atmosphere Model,
238 *Geosci. Model Dev.*, 9, 505-522, doi:10.5194/gmd-9-505-2016, 2016.
239
240 Wang, H., R. C. Easter, P. J. Rasch, M. Wang, X. Liu, S. J. Ghan, Y. Qian, J.-H.
241 Yoon, P.-L. Ma, and V. Vinoj (2013), Sensitivity of remote aerosol distributions to
242 representation of cloud-aerosol interactions in a global climate model, *Geosci.
243 Model Dev.*, 6, 765–782, doi:10.5194/gmd-6-765-2013.
244
245 Wang, H., P. J. Rasch, R. C. Easter, B. Singh, R. Zhang, P.-L. Ma, Y. Qian, S. J.
246 Ghan, and N. Beagley (2014), Using an explicit emission tagging method in
247 global modeling of source-receptor relationships for black carbon in the Arctic:
248 Variations, sources, and transport pathways, *J. Geophys. Res. Atmos.*, 119,
249 12,888–12,909, doi:10.1002/2014JD022297.
250
251 Ghan, S. J., and R. A. Zaveri (2007), Parameterization of optical properties for
252 hydrated internally mixed aerosol, *J. Geophys. Res.*, 112, D10201,
253 doi:10.1029/2006JD007927.
254
255 Bond, T. C., and R. W. Bergstrom, Light absorption by carbonaceous particles: An
256 investigative review, *Aerosol. Sci. Technol.*, 40, 27–67,
257 doi:10.1080/02786820500421521, 2006.
258
259 Koepke, M. H. P., and I. Schult, Optical properties of aerosols and clouds: The
260 software package opac, *Bull. Am. Meteorol. Soc.*, 79, 831–844, 1998,
261 doi:10.1175/1520-0477(1998)079<0831:OPOAAC>2.0.CO;2.
262
263 Wang, M., S. Ghan, M. Ovchinnikov, X. Liu, R. Easter, E. Kassianov, Y. Qian, and H.
264 Morrison (2011), Aerosol indirect effects in a multi-scale aerosol-climate model
265 PNNL-MMF, *Atmos. Chem. Phys.*, 11, 5431–5455,
266 doi:10.5194/acp-11-5431-2011.
267

268 He, C., Li, Q., Liou, K.-N., Qi, L., Tao, S., and Schwarz, J. P.: Microphysics-based
269 black carbon aging in a global CTM: constraints from HIPPO observations and
270 implications for global black carbon budget, *Atmos. Chem. Phys.*, 16, 3077-3098,
271 doi:10.5194/acp-16-3077-2016, 2016b.
272
273 Oshima, N., M. Koike, Y. Zhang, Y. Kondo, N. Moteki, N. Takegawa, and Y. Miyazaki
274 (2009), Aging of black carbon in outflow from anthropogenic sources using a
275 mixing state resolved model: Model development and evaluation, *J. Geophys.*
276 *Res.*, 114, D06210, doi:10.1029/2008JD010680.
277
278 Schuster, G. L., Dubovik, O., Arola, A., Eck, T. F., and Holben, B. N.: Remote sensing
279 of soot carbon – Part 2: Understanding the absorption Ångström exponent,
280 *Atmos. Chem. Phys.*, 16, 1587-1602, doi:10.5194/acp-16-1587-2016, 2016.
281
282 Kurokawa, J., Ohara, T., Morikawa, T., Hanayama, S., Janssens-Maenhout, G.,
283 Fukui, T., Kawashima, K. and Akimoto, H.: Emissions of air pollutants and
284 greenhouse gases over Asian regions during 2000–2008: Regional Emission
285 inventory in ASia (REAS) version 2, *Atmospheric Chem. Phys.*, 13(21), 11019–
286 11058, 2013.
287
288 Qin, Y. and Xie, S. D.: Spatial and temporal variation of anthropogenic black carbon
289 emissions in China for the period 1980–2009, *Atmos Chem Phys*, 12(11), 4825–
290 4841, doi:10.5194/acp-12-4825-2012, 2012.
291
292 Zhao, Y., Zhang, J. & Nielsen, C. P. 2013. The effects of recent control policies on
293 trends in emissions of anthropogenic atmospheric pollutants and CO₂ in China.
294 *Atmos. Chem. Phys.*, 13, 487-508.
295
296 Lu, Z., Zhang, Q. & Streets, D. G. 2011. Sulfur dioxide and primary carbonaceous
297 aerosol emissions in China and India, 1996–2010. *Atmos. Chem. Phys.*, 11,
298 9839-9864.
299
300 Huo, H., Lei, Y., Zhang, Q., Zhao, L. & He, K. 2012. China's coke industry: Recent
301 policies, technology shift, and implication for energy and the environment. *Energy*
302 *Policy*, 51, 397-404.
303
304 Klimont, Z., Kupiainen, K., Heyes, C., Purohit, P., Cofala, J., Rafaj, P.,
305 Borken-Kleefeld, J. and Schöpp, W.: Global anthropogenic emissions of
306 particulate matter including black carbon, *Atmospheric Chem. Phys. Discuss.*, 1–
307 72, doi:10.5194/acp-2016-880, 2016.
308
309
310
311

315
316 Yang et al. investigated the BC source attributions (or more specifically, region
317 attributions) in China with a source-tagging technique by employing a global climate
318 model, NCAR's Community Earth System Model. They found out that BC emissions
319 from local (inside China) and non-local (outside China) are both generally important
320 contributions to air quality in different regions of China, BC outflow from East Asia and
321 direct radiative forcings. Overall, this paper is a helpful addition to our community that
322 attempts to improve our understanding of BC source-receptor relationship. This paper
323 generally reads well and is within the scope of ACP. However, before it can be
324 accepted for publication in ACP, I have several comments that need to be properly
325 addressed.

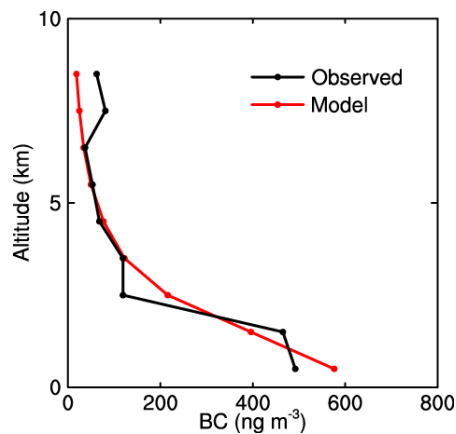
326
327 Major comments:

328
329 An important part of this study was to quantify the BC source contributions to
330 trans-boundary and trans-pacific transport. In terms of model performance
331 evaluation, this study only validated model simulations with observed BC surface
332 concentrations from CAWNET and AAOD from AERONET over China. We don't
333 know the efficiency of BC outflow from East Asia. In this paper, it obviously missed
334 the evaluations of model simulated vertical profiles of BC against aircraft campaign
335 observations, e.g. A-FORCE and HIPPO, which should be employed to compare with
336 model simulations.

337
338 Response:

339 Thanks for the suggestion. The simulated BC vertical profile in CAM5 has been
340 extensively evaluated in many previous studies. Liu et al. (2012) compared the
341 observed and simulated BC vertical profiles in the tropics, middle latitudes, and high
342 latitudes from six aircraft campaigns: AVE Houston (NASA Houston Aura Validation
343 Experiment), CR-AVE (NASA Costa Rica Aura Validation Experiment), TC4 (Tropical
344 Composition, Cloud and Climate Coupling), CARB (NASA initiative in collaboration
345 with California Air Resources Board), ARCTAS (NASA Arctic Research of the
346 Composition of the Troposphere from Aircraft and Satellite), and ARCPAC (NOAA
347 Aerosol, Radiation, and Cloud Processes affecting Arctic Climate), as well as BC
348 vertical profiles over the Arctic Ocean and the remote Pacific Ocean during the
349 HIPPO (HIAPER Pole-to-Pole Observations) campaign. They found that measured
350 BC mixing ratios showed a strong gradient from the boundary layer to the free
351 troposphere in the tropics, while modeled BC mixing ratios showed a smaller
352 decrease with altitude in the free troposphere, thus overestimating observations
353 above 500 hPa. Compared to HIPPO campaign, the CAM5 model captured the
354 vertical variations of BC mixing ratio reasonably well in the SH high latitudes and NH

355 and SH mid-latitudes. However, modeled BC showed less vertical reduction in the
 356 tropics, thus significantly overestimating BC in the upper troposphere.
 357 Wang et al. (2013) implemented in CAM5 a unified treatment of wet removal and
 358 vertical transport of aerosols by convection, which included an explicit secondary
 359 activation of aerosols being laterally entrained into convective clouds above cloud
 360 base. The comparisons between the new CAM5 simulated vertical profiles of BC
 361 mass mixing ratios and the HIPPO and the field campaign aircraft observations
 362 showed a substantial improvement in the simulation of BC in mid- and upper
 363 troposphere, where the excessive BC was significantly reduced. All of these key
 364 model improvements by Wang et al. (2013) have been included in the version of
 365 CAM5 being used in the present study. Therefore, we did not duplicate the evaluation
 366 of BC vertical profiles with HIPPO observation. We have now revised the description
 367 before model evaluation to make it clear, as “The simulations of aerosols, especially
 368 BC, using CAM5 have been extensively evaluated against observations including
 369 aerosol mass and number concentrations, vertical profiles, aerosol optical properties,
 370 aerosol deposition, and cloud-nucleating properties in several previous studies (e.g.,
 371 Liu et al., 2012, 2016; H. Wang et al., 2013; Ma et al., 2013b; Jiao et al., 2014; Qian
 372 et al., 2014; R. Zhang et al., 2015a,b).”
 373 In addition, as the referee suggested, we have added a comparison of the
 374 simulated BC vertical profile with A-FORCE measurements over East Asia (see
 375 Figure S2). The model successfully reproduces the vertical profile of BC. The bias is
 376 relatively small. We have also added a relevant discussion to the revised manuscript,
 377 as “Figure S2 compares the observed and simulated vertical profiles of BC
 378 concentrations in the East-Asian outflow region. The model successfully reproduces
 379 the vertical profile of BC that was measured in March–April 2009 during the
 380 A-FORCE field campaign and reported by Oshima et al. (2012).”
 381



382
 383
 384 Figure S2. Observed and simulated mean vertical profiles of BC concentrations in the
 385 East-Asian outflow region. The observed BC profile is from the A-FORCE field

386 campaign conducted over the Yellow Sea, the East China Sea, and the western
387 Pacific Ocean in March–April 2009 (Oshima et al., 2012).

388
389
390

391 Other minor comments:

392

393 Line 124: the reference Hoesly et al., 2016 is missing in the reference list.

394 **Response:**

395 The paper is still in preparation. A draft can be made available to referees upon
396 request.

397

398 Line 162: A brief description of dry/wet deposition scheme for BC in CAM is lacking
399 here, especially the wet scavenging and how it is improved following H. Wang et al.
400 (2013).

401 **Response:**

402 Aerosol dry deposition velocities are calculated using the Zhang et al. (2001)
403 parameterization. The wet deposition of aerosols in our CAM5 model includes
404 in-cloud wet removal (i.e., activation of interstitial aerosols to cloud-borne particles
405 followed by precipitation scavenging) and below-cloud wet removal (i.e., capture of
406 interstitial aerosol particles by falling precipitation particles) for both stratiform and
407 convective clouds. Aerosol activation is calculated with the parameterization of
408 Abdul-Razzak and Ghan (2000) for stratiform cloud throughout the column and
409 convective cloud at cloud base, while the secondary activation above convective
410 cloud base has a simpler treatment with an assumed maximum supersaturation in
411 convective updrafts (H. Wang et al., 2013). The unified treatment for convective
412 transport and aerosol wet removal along with the explicit aerosol activation above
413 convective cloud base was developed by H. Wang et al. (2013) and included in the
414 CAM5 version being used in this study. As discussed in the response to the major
415 comment, this implementation reduces the excessive BC aloft and better simulates
416 observed BC concentrations in the mid- to upper-troposphere.

417 We have now added these descriptions to the Methods section.

418

419 Line 334-336: This sentence should be corrected as “AI derived from Total Ozone
420 Mapping Spectrometer (TOMS) measurements also shows similar pattern as
421 simulate AAOD (Fig. S2).”

422 **Response:**

423 Corrected.

424

425 Line 339-344: What’s the assumption here? Why the ratio of AAOD to AI should be
426 the same between western and eastern China? What is the role of dust here in
427 assisting the speculation?

428 **Response:**

429 Based on the comparison of AAOD between the model simulation and
430 AERONET, we found that the model reproduced well the observed AAOD over
431 eastern China. Therefore, we assume that the ratio of modeled AAOD and satellite AI
432 (indicator for absorbing aerosols) is correct over eastern China. The AAOD/AI over
433 eastern China is much larger than western China, suggesting that the ratio AAOD/AI
434 is lower than the true value and AAOD or BC burden is likely underestimated in the
435 model. Both AAOD and AI represent absorbing aerosols, the ratio of AAOD to AI may
436 be different but similar between different regions in China. The difference in the ratio
437 between eastern and western China is quite large, suggesting the existence of a
438 significant bias. This is consistent with the contrast of biases in near-surface BC
439 concentrations between the two regions (shown in Fig. 3). However, both BC and
440 dust can contribute to AAOD and AI. Potential biases in the modeled dust could also
441 lead to the inconsistency of AAOD/AI between eastern and western China.

442 We have revised the description to make it clear, as "If we assume that the
443 simulated AAOD do not have large biases over eastern China based on the
444 evaluation against observations shown above (Fig. 3b and Table S3), then this
445 difference hints a possible underestimation of BC column burden in the model over
446 the western regions. However, it is difficult to draw a firm conclusion, given the likely
447 differential role of dust in eastern vs western China. This differential likely also
448 contributes to AAOD biases in modeling dust and may also impact biases in the
449 satellite derived AI values."

450
451 Line 424-426: I think BC emissions from SC are also important for the column
452 burdens over continental China in some seasons (e.g. JJA and SON), which needs to
453 be outlined as well.

454 Response:

455 Thanks for the suggestion. We have now added the SC contribution to column
456 burden, as "Column burdens of BC averaged over continental China mainly originate
457 from emissions in North China, South China and outside China, with relative
458 contributions ranging from 35–46%, 14–21% and 12–30%, respectively."

459
460 Line 443: "Figure S4a" should be replaced with "Fig. S5a".

461 Response:

462 Corrected.

463
464 Line 443-463: It is helpful for the authors to make supplemental plots showing the
465 anomalous winds during polluted days that favor the accumulation of pollutants over
466 each region.

467 Response:

468 We did show in Fig. 8 the anomalous winds at 850 mb between polluted and
469 normal days for each region during winter.

470
471 Line 505-509: Why the authors only choose the latitude range along longitude 150°E,
472 not a domain covering East China Sea and West Pacific to quantitatively assess the

473 BC contributions from China and outside China, similar to that impact over West
474 United States?

475 Response:

476 The outflow of aerosols, defined as the column-integrated aerosol flux or
477 concentration along a vertical cross-section, is used to characterize the export of BC
478 from East Asia. This calculation of outflow follows previous studies and thus is
479 comparable to the results in these studies (Hadley et al., 2007; Matsui et al., 2013;
480 Yang et al., 2015). In addition, using a region around 150°E does not change the
481 values significantly (e.g., contribution from China changes from 55% for the outflow
482 at 150°E to 56% for an average over 145–155°E). We don't mean to assess the
483 contributions from China and outside China to air quality over this region.

484
485 Line 509-510: I get lost here. It is not clear to me that 58% contribution from China
486 emissions is for outflow or something else. Authors need to clarify this.

487 Response:

488 Clarified as "The yearly contribution from emissions from China to outflow from
489 East Asia in this study is 59%, similar to the contribution of 61% in Matsui et al. (2013)
490 calculated based on eastward BC mass flux using WRF-CMAQ model with INTEX-B
491 missions."

492
493 Line 531-538: I think the authors should list a table to compare your results with other
494 studies, including annual BC emission budgets, burden, lifetime, DRF and DRF
495 efficiency.

496 Response:

497 Thanks the suggestion. We have added Table S5 to compare these values with
498 previous studies.

499 We have also added a discussion of this comparison in the manuscript, as "The
500 total DRF of BC averaged over continental China simulated in this study is 2.20 W
501 m⁻², larger than 0.64–1.55 W m⁻² in previous studies (Wu et al., 2008; Zhuang et al.,
502 2011; Li et al., 2016), probably due to the different emissions in the time periods of
503 study, as shown in Table S5." And "The annual mean and regional mean DRF
504 efficiency in China is 0.88 W m⁻² Tg⁻¹, within the range of 0.41–1.55 W m⁻² Tg⁻¹ from
505 the previous studies (Table S5)."

506
507 **Table S5.** Comparison of the simulated annual mean emission, burden, DRF and
508 DRF efficiency in China in this study with the values reported in three previous
509 studies.

510

Reference	Model	Year	Emission in China (Gg yr ⁻¹)	Burden (mg m ⁻²)	DRF (Wm ⁻²)	DRF efficiency (W m ⁻² Tg ⁻¹)
Wu et al. (2008)	RegCM3	2000	1005	0.55–1.42	0.64–1.55	0.64–1.55
Zhuang et al. (2011)	RegCCMS	2006	1811	1.12	0.75	0.41
Li et al. (2016)	GEOS-Chem	2010	1840		1.22	0.66
This study	CESM	2010–2014	2497	1.61	2.20	0.88

511
512
513
514 Line 654-655: Other modeling studies also found model low bias over China using
515 CAWNNET, e.g. Huang et al., 2013; Wang et al., 2014, which can be referenced here.
516 Huang, Y., S. Wu, M. K. Dubey, and N. H. F. French, Impact of aging mechanism on
517 model simulated carbonaceous aerosols, *Atmos. Chem. Phys.*, 13, 6329–6343,
518 doi:10.5194/acp-13- 6329-2013, 2013.
519 Wang, Q., D.J. Jacob, J.R Spackman, A.E. Perring, J.P. Schwarz, N. Moteki, E.A.
520 Marais, C. Ge, J. Wang and S.R.H. Barrett, Global budget and radiative forcing of
521 black carbon aerosol: constraints from pole-to-pole (HIPPO) observations across the
522 Pacific, *J. Geophys. Res.*, 119, 195- 206, 2014.
523 **Response:**
524 **Added.**
525
526 Line 669: “and” is missing between “modeled” and “observed”.
527 **Response:**
528 **Added.**
529
530
531 **References:**
532 **Zhang, L. M., Gong S. L., Padro J. and Barrie L.: A size-segregated particle dry**
533 **deposition scheme for an atmospheric aerosol module, *Atmos. Environ.*, 35,**
534 **549-560, doi:10.1016/S1352-2310(00)00326-5 ,2001.**
535
536 **Abdul-Razzak, H., and Ghan S. J.: A parameterization of aerosol activation: 2.**
537 **Multiple aerosol types, *J. Geophys. Res.*, 105, 6837–6844,**
538 **doi:10.1029/1999JD901161, 2000.**
539
540 **Wang, H., R. C. Easter, P. J. Rasch, M. Wang, X. Liu, S. J. Ghan, Y. Qian, J.-H.**
541 **Yoon, P.-L. Ma, and V. Vinoj (2013), Sensitivity of remote aerosol distributions to**
542 **representation of cloud-aerosol interactions in a global climate model, *Geosci.***
543 **Model Dev.**, 6, 765–782, doi:10.5194/gmd-6-765-2013.
544
545 **Hadley, O. L., V. Ramanathan, G. R. Carmichael, Y. Tang, C. E. Corrigan, G. C.**
546 **Roberts, and G. S. Mauger (2007), Trans-Pacific transport of black carbon and**
547 **fine aerosols ($D < 2.5 \mu\text{m}$) into North America, *J. Geophys. Res.*, 112, D05309,**
548 **doi:10.1029/2006JD007632.**
549
550 **Matsui, H., M. Koike, Y. Kondo, N. Oshima, N. Moteki, Y. Kanaya, A. Takami, and M.**
551 **Irwin (2013), Seasonal variations of Asian black carbon outflow to the Pacific:**
552 **Contribution from anthropogenic sources in China and biomass burning sources**
553 **in Siberia and Southeast Asia, *J. Geophys. Res. Atmos.*, 118, 9948–9967,**
554 **doi:10.1002/jgrd.50702.**

555
556 Yang Y., H. Liao, and S. Lou (2015), Decadal trend and interannual variation of
557 outflow of aerosols from East Asia: Roles of variations in meteorological
558 parameters and emissions, *Atmos. Environ.*, 100, 141-153,
559 doi:10.1016/j.atmosenv.2014.11.004.
560
561 Oshima, N., Y. Kondo, Moteki N., Takegawa N., Koike M., Kita K., Matsui H., Kajino
562 M., Nakamura H., Jung J. S., and Kim Y. J.: Wet removal of black carbon in Asian
563 outflow: Aerosol Radiative Forcing in East Asia (A-FORCE) aircraft campaign, *J.*
564 *Geophys. Res.*, 117, D03204, doi:10.1029/2011JD016552, 2012.
565
566 Huang, Y., S. Wu, M. K. Dubey, and N. H. F. French, Impact of aging mechanism on
567 model simulated carbonaceous aerosols, *Atmos. Chem. Phys.*, 13, 6329–6343,
568 doi:10.5194/acp-13- 6329-2013, 2013.
569
570 Wang, Q., D.J. Jacob, J.R Spackman, A.E. Perring, J.P. Schwarz, N. Moteki, E.A.
571 Marais, C. Ge, J. Wang and S.R.H. Barrett, Global budget and radiative forcing of
572 black carbon aerosol: constraints from pole-to-pole (HIPPO) observations across
573 the Pacific, *J. Geophys. Res.*, 119, 195- 206, 2014.
574
575
576
577

581
582
583 This study quantified source contributions of black carbon (BC) mass concentrations,
584 trans-Pacific transport of BC, and direct radiative forcing of BC from seven regions in
585 China using the Community Earth System Model with a source-tagging technique.
586 The authors showed that BC concentrations were dominated by local emissions for
587 regions with high emissions (e.g., North China, South China), whereas non-local
588 emissions were important for regions with low emissions (e.g., Northwest China,
589 Tibetan Plateau). They also showed that emissions from China and other regions
590 were equally important for the BC outflow from East Asia and that emissions from
591 China would be important for air quality in western United States. The annual mean
592 direct radiative forcing of BC in China in their simulations was 2.3 W m^{-2} , and the
593 contribution from emissions in China was estimated to be 66%.

594
595 The purpose of this study is interesting and the results obtained in this study are
596 important to understand BC behavior in the atmosphere over East Asia. I think the
597 authors should describe several points (shown below) more clearly, but overall the
598 manuscript is written well and is suitable for the publication of this journal.

599
600 Major comments:

601
602 (1) Importance of BC in air quality problems

603 The authors sometimes use BC as an indicator of pollution (or air quality) in China
604 (Lines 39-40, Lines 101-102, Lines 429-431, and Lines 571-572). However, I think it
605 is questionable whether the concentrations and/or source contributions of BC can be
606 used to represent those of total aerosols. Inorganic and organic species are dominant
607 in China during polluted days, and spatial/temporal variations and source
608 contributions of these species are largely different from those of BC because spatial
609 distributions of emissions (e.g., BC v.s. SO₂) and formation processes (primary v.s.
610 secondary) are considerably different. For example, Matsui et al. (2009) showed that
611 primary aerosols around Beijing were controlled by emissions within 100 km around
612 Beijing within the preceding 24 h, while emissions as far as 500 km and within the
613 preceding 3 days were found to affect secondary aerosols. Therefore, it is not always
614 correct to extend the results of BC (e.g., source contributions) to the discussions on
615 pollution and air quality because inorganic and organic species could have larger
616 contributions from non-local emissions than BC. Please consider this point and
617 describe the limitation of using BC results only in the discussions of air quality
618 problems. In addition, please show the percentage of BC mass to total mass (PM_{2.5})
619 in China in the manuscript.

620 **Response:**

621 We agree with the referee that by no means BC can represent the total PM_{2.5} in
622 air quality problems, which is not the focus of this study. We have added a paragraph
623 in the discussion section to describe the limitation of using BC as a tracer for air
624 pollution, as “In this study, BC is used as an indicator of pollution (or air quality) in
625 China. Although BC is often co-emitted with other species, such as primary organic
626 matter, organic gases and sulfuric gases, source-receptor relationship of BC may not
627 fully represent that of total aerosols. The contribution of BC to total near-surface
628 PM_{2.5} concentrations averaged over China is less than 10%. Other aerosols, such as
629 sulfate, are dominant in China during polluted days. The spatio-temporal variations
630 and source contributions of these species are largely different from those of BC
631 because spatial distributions of emissions (e.g., SO₂) and formation processes can
632 be considerably different. For example, Matsui et al. (2009) showed that primary
633 aerosols around Beijing were determined by emissions within 100 km around Beijing
634 within the preceding 24 hours, while emissions as far as 500 km and within the
635 preceding 3 days were found to affect secondary aerosols in Beijing. Thus, the
636 secondary aerosols could have larger contributions from non-local emissions than
637 BC. BC concentrations are highest in winter over China due to higher emissions,
638 while sulfate concentrations reach maximum in summer when the strong sunlight and
639 high temperature favor the sulfate formation. Therefore, knowing the accurate source
640 attributions of air pollution in China requires source tagging for more aerosol species,
641 such as sulfate.”

642

643 (2) Treatment of optical property and CCN activity of BC (Lines 151-169)

644 I could not find the description on the treatment of optical property (well-mixed, core-
645 shell, or others) and CCN activity (conversion from hydrophobic to hydrophilic BC) of
646 BC in the MAM3 model. I assume that well-mixed optical treatment is used to
647 calculate BC absorption and that all BC particles are treated as hydrophilic BC in
648 MAM3. Please describe the treatment of optical property and CCN activity of BC in
649 the manuscript, and add some description on the potential impact (uncertainty) of
650 these treatments on the estimation of BC concentrations, trans-Pacific transport of
651 BC, AAOD, and direct radiative forcing of BC and their source contributions.

652 Response:

653 Thanks for the suggestion. We have added more information regarding the
654 treatment of BC in the model to the Methods section and also added a paragraph
655 discussing the potential influence in the Methods and Conclusions and Discussions
656 section, shown as below:

657 Aerosol optical properties for each mode are parameterized according to Ghan
658 and Zaveri (2007). Refractive indices for aerosols are taken from the OPAC (optical
659 properties for aerosols and clouds) software package (Koepke and Schult, 1998), but
660 for BC at solar wavelengths the values are updated from Bond and Bergstrom (2006).
661 In MAM3, the aging process of BC is neglected by assuming the immediate mixing of
662 BC with other aerosol species.

663 BC aging in the atmosphere is important for BC concentration and its optical
664 properties, which transforms BC from hydrophobic aggregates to hydrophilic particles

665 coated with soluble materials. He et al. (2015, 2016a) found that BC optical properties
666 varied by a factor of two or more due to different coating structures during BC aging
667 process based on their theoretical and experimental intercomparison. Oshima et al.
668 (2009) and He et al. (2016b) pointed out that the use of various microphysical BC
669 aging schemes could significantly improve simulations of BC concentrations
670 compared to the simplified aging parameterizations. Liu et al. (2012) also reported
671 that the wet removal rate of BC simulated in standard CAM5 is 60% higher than
672 AeroCom multi-model mean due to the rapid or instantaneous aging of BC. H. Wang
673 et al. (2013) showed that the explicit treatment of BC aging process with slow aging
674 assumptions in CAM5 could significantly increase BC lifetime and the efficiency of BC
675 long-range transport. In the three-mode aerosol module (MAM3) of CAM5 used in this
676 study, the aging process of BC is neglected by assuming the immediate internal
677 mixing of BC with other aerosol species in the same mode. This assumption could
678 lead to an overestimation of wet removal of BC and, therefore, an underestimation of
679 BC concentrations, absorption optical depth (Fig. 3) and direct radiative forcing. In
680 addition, the internally-mixed optical treatment in CAM5 could also cause bias in BC
681 absorption calculation. However, H. Wang et al. (2014) examined source-receptor
682 relationships for BC under the different BC aging assumptions and found that the
683 quantitative source attributions varied slightly while the qualitative source-receptor
684 relationships still hold. Therefore, although the magnitude of simulated BC and its
685 optical properties could be underestimated due to the instantaneous aging of BC and
686 uncertainty in coating structures, we expect that the aging treatment in MAM3 of
687 CAM5 should not influence the qualitative source attributions examined in this study.

688
689

690 Other comments:

691

692 (3) Line 70

693 Please describe the reason of the faster regional removal.

694 Response:

695 Revised as "BC in East Asia has a shorter lifetime than the global mean value
696 due to a faster regional removal (H. Wang et al., 2014), likely associated with a strong
697 precipitation scavenging near sources and along the transport pathways over the
698 Pacific Ocean."

699

700 (4) Lines 168-169

701 Please clarify the definition of the direct radiative forcing of BC. Is this calculated from
702 the difference of two radiative transfer calculations with and without BC for the
703 clear-sky condition?

704 Response:

705 Revised as "Direct radiative forcing of BC is calculated as the difference in the
706 top-of-the-atmosphere net radiative fluxes with and without BC for the all-sky
707 condition following Ghan (2013)."

708

709 (5) Lines 182-204

710 Please show the difference of BC emission fluxes between the emission inventory
711 used in this study and other emission inventories (e.g., INTEX-B, HTAP). The values
712 are shown later (at Lines 534-538), but I think it is better to show them here. In
713 addition, please add some comments on the impact of larger values of BC emissions
714 in this study on the estimation of source contributions of BC. Can you add the values
715 of BC emissions from outside China (e.g., India, Southeast Asia, Japan, Korea) to
716 Figure 1b?

717 Response:

718 We have added Table S1 to compare the anthropogenic emissions used in this
719 study with emissions from some previous studies. The anthropogenic emissions of
720 BC in China in 2010–2014 are larger than those used in the previous studies for
721 earlier years, partly as a result of the rapid increasing trend of BC in China during
722 recent years. The higher emissions likely lead to higher concentrations and direct
723 radiative forcing, and source contributions of BC in China, compared to the values
724 reported in these studies. We have added these descriptions in the Methods section.

725 We also revised Fig. 1 to include BC emissions from outside China. Emissions at
726 regional scale are summarized here instead of Country level because the model
727 resolution is a bit coarse to characterize emissions by countries. Total BC emissions
728 from neighboring regions including rest of East Asia (REA, with China excluded),
729 South Asia (SAS), Southeast Asia (SEA), and Russia/Belarusia/Ukraine (RBU) are
730 shown in Figure 1c. These source regions outside China are consistent with source
731 regions defined in the second phase of Hemispheric Transport of Air Pollution
732 (HTAP2). South Asia and Southeast Asia have relatively high emissions. They may
733 dominate the contribution to concentrations and direct radiative forcing of BC in
734 China, especially southern and western China, from foreign sources through
735 long-range transport. We have also added these in the Methods section. We did not
736 compare the emissions outside China with other studies, which is beyond the scope
737 of this study. However, the comparison of CEDS emissions with other emission
738 inventories can be found in Hoesly et al. (2017), which includes detailed information
739 of the CEDS emissions and will be submit very soon.

740 We also added a paragraph about uncertainty in BC emissions in the
741 Conclusions and discussions section, as "Uncertainty in China BC emissions has
742 been estimated as –43% to 93% by Lu et al. (2011), –50% to 164% by Qin and Xie
743 (2012), ±176% by Kurokawa et al. (2013), and –28 to 126% by Zhao et al. (2013).
744 The BC emissions estimates used here for China in 2010 are 40% higher than those
745 of Zhao et al. (2013) and Lu et al. (2011) and 30% higher than Klimont et al. (2016), in
746 large part due to a higher estimate of BC emissions from coal coke production.
747 Emissions from coke production are particularly uncertain given that "there are no
748 measurements for PM2.5 and BC emissions" (Huo et al. 2012) available to guide
749 inventory estimates. Total rest of the world emissions other than China, which appear
750 to be a major contributor to burdens over western regions, are within 1% of those
751 from Klimont et al. (2016)."

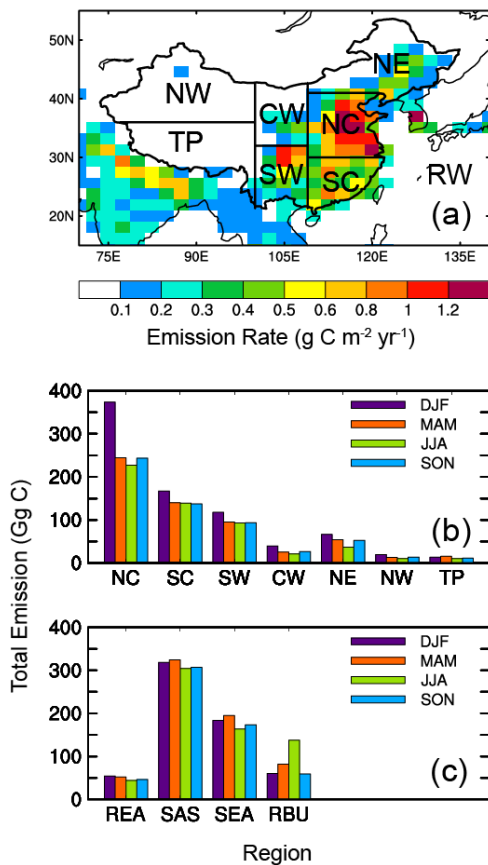
752

753
754
755
756
757

Table S1. Comparison of CEDS annual mean anthropogenic BC emissions in China with those used in other studies

	Year	Anthropogenic emission in China (Gg/yr)
CEDS		
(Hoesly et al., 2016; this study)	2010–2014	2467
MIX (Li et al., 2017)	2010	1765
HTAP V2.2 (Janssens-Maenhout et al., 2015)	2010	1741
Lu et al. (2011)	2010	1751
Qin and Xie (2012)	2009	1764
Wang et al. (2012)	2007	1879
INTEX-B (Zhang et al., 2009)	2006	1811

758



759
 760
 761
 762
 763
 764
 765
 766
 767
 768
 769
 770
 771
 772
 773
 774

Figure 1. (a) Spatial distribution of annual mean total emissions (anthropogenic plus biomass burning, units: $\text{g C m}^{-2} \text{ yr}^{-1}$) of black carbon (BC) averaged over 2010–2014. The geographical BC source regions are selected as North China (NC, 109°E–east boundary, 30°–41°N), South China (SC, 109°E–east boundary, south boundary–30°N), Southwest China (SW, 100°–109°E, south boundary–32°N), Central-West China (CW, 100°–109°E, 32°N–north boundary), Northeast China (NE, 109°E–east boundary, 41°N–north boundary), Northwest China (NW, west boundary–100°E, 36°N–north boundary), and Tibetan Plateau (TP, west boundary–100°E, south boundary–36°N) in China and regions outside of China (RW, rest of the world). (b) Seasonal mean total emissions (units: Gg C , $\text{Gg} = 10^9\text{g}$) of BC from the seven BC source regions in China and (c) emissions from rest of East Asia (REA, with China excluded), South Asia (SAS), Southeast Asia (SEA), and Russia/Belarus/Ukraine (RBU).

775 (6) Lines 261-263

776 You can show the contributions from outside China quantitatively from the tagged
777 simulation results.

778 Response:

779 We show the quantitative contributions from outside China in the Results section.
780 It is not appropriate to directly compare the contribution to surface concentrations and
781 that to column burden. Therefore, we decide to remove this sentence to avoid
782 duplication and potential misunderstanding.

783

784 (7) Line 281

785 Please describe the reason of BC underestimation by up to a factor of 20.

786 Response:

787 We have discussed possible causes of this underestimation of BC in the following
788 part of the Results section and in the Discussion section as well:

789 "Note that the model largely underestimates BC concentrations over China,
790 compared to the observation, which has also been reported in many previous studies
791 using different models and different emission inventories (e.g., Liu et al., 2012; Fu et
792 al., 2012; Huang et al., 2013; H. Wang et al., 2013; Q. Wang et al., 2014; R. Wang et
793 al., 2014; Li et al., 2016). One possible reason is that in situ measurements are point
794 observations, while the model does not treat the subgrid variability of aerosols and
795 assumes aerosols are uniformly distributed over the grid cell. R. Wang et al. (2014)
796 found a reduction of negative bias (from -88% to -35%) in the modeled surface BC
797 concentrations when using high-resolution emissions and modeling at 0.5° X 0.7°
798 resolution. They find, however, that modeling over the North China Plain at an even
799 higher resolution of 0.1°, further reduced the surface concentration bias there from
800 29% to 8%. This result indicates that the siting of observational stations can result in
801 an artificial bias when comparing with relatively coarse model results. Further
802 investigation of this siting/resolution bias is warranted, including investigation on
803 whether this type of bias might extend, presumably to a lesser extent, also to AOD
804 measurements.

805 Further reasons that could contribute to this bias are emission underestimation or
806 inaccurate aerosol processes in the model. Given that the differences between
807 modeled and observed AOD over eastern China are relatively small (-6%), we
808 conclude that, given current evidence, the total amount of atmospheric BC in these
809 simulations is reasonable at least in this sub-region.

810 Over eastern China, the BC concentrations are dominated by local emissions in
811 this study, with local contribution of 58–94%. The underestimation of simulated BC
812 concentrations over eastern China is more likely due to either underestimation of
813 local emissions, too much aerosol removal within these regions, or resolution bias
814 between observations and model grids. Over western China, 18–78% of the BC
815 originates from emissions outside China. Thus biases of simulated BC concentrations
816 could also come from underestimation of emissions outside China and or too much
817 removal of BC during long-range transport. Satellite data are a promising method to
818 validate modeling and emissions inventories, given that they do not depend on the

819 location of observing stations, providing more uniform spatial coverage. A
820 comparison of modeled AAOD and satellite aerosol index (AI) provides an indication
821 that the modeled burden in western China is underestimated, although the role of
822 dust needs to be better characterized.”

823
824 (8) Line 343

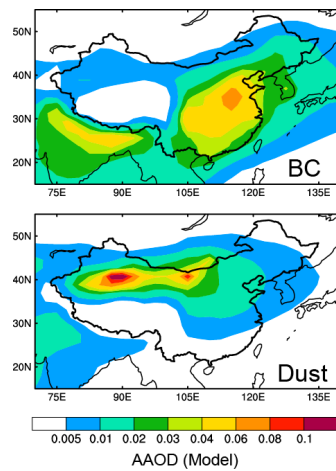
825 I cannot find large sources of BC in Northwest China in Figure 1a. Does the
826 description here mean that there may be large sources of BC which are not
827 considered in the emission inventory? Can you show the contribution of BC and dust
828 to AAOD (in model) over this region? I think dust is dominant over this region.

829 Response:

830 Yes, underestimation of emissions over Northwest China could be part of the
831 story. In the source attribution analysis, we found that emissions from outside China
832 also contribute substantially to BC concentrations in Northwest China. Therefore the
833 underestimation in BC concentrations could also come from low biases in emissions
834 outside China or too much removal during along the transport pathways in the model.

835 Dust AAOD is indeed dominant over Northwest China (Fig. A). Potential biases in
836 dust simulation could also lead to the difference in AAOD between model and
837 observation. That is why we noted the potential bias from dust simulation, as
838 “However, it is difficult to draw a firm conclusion, given the likely differential role of
839 dust that also contributes to AAOD and AI, biases in modeling dust, and possible
840 biases in the satellite derived AI values.” And “A comparison of modeled AAOD and
841 satellite aerosol index (AI) provides an indication that the modeled burden in western
842 China is underestimated, although the role of dust needs to be better characterized.”

843



844
845 Figure A. Simulated annual mean AAOD of BC and dust.

846
847 (9) Lines 667-669

848 Related to the comment (2), is an internally-mixed treatment used in the calculations
849 of AAOD? If so, AAOD should be lower (underestimated more) when more realistic
850 BC mixing state treatment is used in the optical calculations.

851 Response:

852 CAM5 assumes internal mixing between BC and other components in the same
853 mode, but external mixing between modes in the calculations of optical properties of
854 the mixture of aerosol particles. Compared to the more sophisticated shell-core
855 treatment, the current treatment might underestimate the absorption of aerosol. The
856 aerosol mixing state along with the representation of size distribution is still quite
857 uncertain. There is no strong evidence suggesting which one is more realistic, so we
858 prefer not to draw such a conclusion here.

859

860

861

862 References:

863 Matsui, H., et al. (2009), Spatial and temporal variations of aerosols around Beijing in
864 summer 2006: Model evaluation and source apportionment, *J. Geophys. Res.*,
865 114, D00G13, doi:10.1029/2008JD010906.

866

867 Ghan, S. J., and R. A. Zaveri (2007), Parameterization of optical properties for
868 hydrated internally mixed aerosol, *J. Geophys. Res.*, 112, D10201,
869 doi:10.1029/2006JD007927.

870

871 Bond, T. C., and R. W. Bergstrom, Light absorption by carbonaceous particles: An
872 investigative review, *Aerosol. Sci. Technol.*, 40, 27–67,
873 doi:10.1080/02786820500421521, 2006.

874

875 Koepke, M. H. P., and I. Schult, Optical properties of aerosols and clouds: The
876 software package opac, *Bull. Am. Meteorol. Soc.*, 79, 831–844, 1998,
877 doi:10.1175/1520-0477(1998)079<0831:OPOAAC>2.0.CO;2.

878

879 He, C., Liou, K.-N., Takano, Y., Zhang, R., Levy Zamora, M., Yang, P., Li, Q., and
880 Leung, L. R.: Variation of the radiative properties during black carbon aging:
881 theoretical and experimental intercomparison, *Atmos. Chem. Phys.*, 15,
882 11967-11980, doi:10.5194/acp-15-11967-2015, 2015.

883

884 He, C., Takano, Y., Liou, K.-N., Yang, P., Li, Q., and Mackowski, D. W.:
885 Intercomparison of the GOS approach, superposition T- matrix method, and
886 laboratory measurements for black carbon optical properties during aging, *J.*
887 *Quant. Spectrosc. Ra.*, 184, 287–296, doi:10.1016/j.jqsrt.2016.08.004, 2016a.

888

889 He, C., Li, Q., Liou, K.-N., Qi, L., Tao, S., and Schwarz, J. P.: Microphysics-based
890 black carbon aging in a global CTM: constraints from HIPPO observations and

891 implications for global black carbon budget, *Atmos. Chem. Phys.*, 16, 3077-3098,
892 doi:10.5194/acp-16-3077-2016, 2016b.
893
894 Oshima, N., M. Koike, Y. Zhang, Y. Kondo, N. Moteki, N. Takegawa, and Y. Miyazaki
895 (2009), Aging of black carbon in outflow from anthropogenic sources using a
896 mixing state resolved model: Model development and evaluation, *J. Geophys.*
897 *Res.*, 114, D06210, doi:10.1029/2008JD010680.
898
899 Liu, X., et al. (2012), Toward a minimal representation of aerosols in climate models:
900 Description and evaluation in the Community Atmosphere Model CAM5, *Geosci.*
901 *Model Dev.*, 5, 709–739, doi:10.5194/gmd-5-709-2012.
902
903 Liu, X., Ma, P.-L., Wang, H., Tilmes, S., Singh, B., Easter, R. C., Ghan, S. J., and
904 Rasch, P. J.: Description and evaluation of a new four-mode version of the Modal
905 Aerosol Module (MAM4) within version 5.3 of the Community Atmosphere Model,
906 *Geosci. Model Dev.*, 9, 505-522, doi:10.5194/gmd-9-505-2016, 2016.
907
908 Wang, H., R. C. Easter, P. J. Rasch, M. Wang, X. Liu, S. J. Ghan, Y. Qian, J.-H.
909 Yoon, P.-L. Ma, and V. Vinoj (2013), Sensitivity of remote aerosol distributions to
910 representation of cloud-aerosol interactions in a global climate model, *Geosci.*
911 *Model Dev.*, 6, 765–782, doi:10.5194/gmd-6-765-2013.
912
913 Wang, H., P. J. Rasch, R. C. Easter, B. Singh, R. Zhang, P.-L. Ma, Y. Qian, S. J.
914 Ghan, and N. Beagley (2014), Using an explicit emission tagging method in
915 global modeling of source-receptor relationships for black carbon in the Arctic:
916 Variations, sources, and transport pathways, *J. Geophys. Res. Atmos.*, 119,
917 12,888–12,909, doi:10.1002/2014JD022297.
918
919 Ghan, S. J. (2013), Technical Note: Estimating aerosol effects on cloud radiative
920 forcing, *Atmos. Chem. Phys.*, 13, 9971-9974, doi:10.5194/acp-13-9971-2013.
921
922 Li, K., Liao, H., Mao, Y. H., and Ridley, D. A.: Source sector and region contributions
923 to concentration and direct radiative forcing of black carbon in China, *Atmos.*
924 *Environ.*, 124, 351–366, doi:10.1016/j.atmosenv.2015.06.014, 2016.
925
926 Janssens-Maenhout, G., Crippa, M., Guizzardi, D., Dentener, F., Muntean, M.,
927 Pouliot, G., Keating, T., Zhang, Q., Kurokawa, J., Wankmüller, R., Denier van der
928 Gon, H., Kuenen, J. J. P., Klimont, Z., Frost, G., Darras, S., Koffi, B., and Li, M.:
929 HTAP_v2.2: a mosaic of regional and global emission grid maps for 2008 and
930 2010 to study hemispheric transport of air pollution, *Atmos. Chem. Phys.*, 15,
931 11411-11432, doi:10.5194/acp-15-11411-2015, 2015.
932

933 Lu, Z., Zhang, Q., and Streets, D. G.: Sulfur dioxide and primary carbonaceous
934 aerosol emissions in China and India, 1996–2010, *Atmos. Chem. Phys.*, 11,
935 9839-9864, doi:10.5194/acp-11-9839-2011, 2011.
936
937 Qin, Y. and Xie, S. D.: Spatial and temporal variation of anthropogenic black carbon
938 emissions in China for the period 1980–2009, *Atmos. Chem. Phys.*, 12,
939 4825-4841, doi:10.5194/acp-12-4825-2012, 2012.
940
941 Wang, R., Tao, S., Wang, W., Liu, J., Shen, H., Shen, G., Wang, B., Liu, X., Li, W.,
942 Huang, Y., Zhang, Y., Lu, Y., Chen, H., Chen, Y., Wang, C., Zhu, D., Wang, X.,
943 Li, B., Liu, W., Ma, J.: Black carbon emissions in China from 1949 to 2050,
944 *Environ. Sci. Technol.*, 46, 7595-7603, doi:10.1021/es3003684, 2012.
945
946 Zhang, Q., Streets, D. G., Carmichael, G. R., He, K. B., Huo, H., Kannari, A., Klimont,
947 Z., Park, I. S., Reddy, S., Fu, J. S., Chen, D., Duan, L., Lei, Y., Wang, L. T., and
948 Yao, Z. L.: Asian emissions in 2006 for the NASA INTEX-B mission, *Atmos.*
949 *Chem. Phys.*, 9, 5131-5153, doi:10.5194/acp-9-5131-2009, 2009.
950

951 Source attribution of black carbon and its direct radiative forcing
952 in China

953

954

955

956 Yang Yang¹, Hailong Wang^{1*}, Steven J. Smith², Po-Lun Ma¹, Philip J. Rasch¹

957

958

959

960 ¹Atmospheric Science and Global Change Division, Pacific Northwest National
961 Laboratory, Richland, Washington, USA

962 ²Joint Global Change Research Institute, Pacific Northwest National Laboratory,
963 College Park, Maryland, USA

964

965

966 *Correspondence to yang.yang@pnnl.gov and hailong.wang@pnnl.gov

967

968 **Abstract**

969 The source attributions for mass concentration, haze formation, transport, and
970 direct radiative forcing of black carbon (BC) in various regions of China are quantified
971 in this study using the Community Earth System Model (CESM) with a source-tagging
972 technique. Anthropogenic emissions are from the Community Emissions Data System
973 that is newly developed for the Coupled Model Intercomparison Project Phase 6
974 (CMIP6). Over North China where the air quality is often poor, about 90% of
975 near-surface BC concentration is contributed by local emissions. 35% of BC
976 concentration over South China in winter can be attributed to emissions from North
977 China and 19% comes from sources outside China in spring. For other regions in
978 China, BC is largely contributed from non-local sources. We further investigated
979 potential factors that contribute to the poor air quality in China. During polluted days, a
980 net inflow of BC transported from non-local source regions associated with
981 anomalous winds plays an important role in increasing local BC concentrations.
982 BC-containing particles emitted from East Asia can also be transported across the
983 Pacific. Our model results show that emissions from inside and outside China are
984 equally important for the BC outflow from East Asia, while emissions from China
985 account for 8% of BC concentration and 29% in column burden in western United
986 States in spring. Radiative forcing estimated shows that 65% of the annual mean BC
987 direct radiative forcing (2.2 W m^{-2}) in China results from local emissions, and the
988 remaining 35% are contributed by emissions outside of China. Efficiency analysis
989 shows that reduction in BC emissions over eastern China could benefit more on the
990 regional air quality in China, especially in winter haze season.

991 **1. Introduction**

992 Black carbon (BC), as a component of atmospheric fine particulate matter
993 (PM_{2.5}), is harmful to human health (Anenberg et al., 2011; Janssen et al., 2012). In
994 addition to its impact on air quality, as the most efficient light-absorbing
995 anthropogenic aerosols, BC is thought to exert a substantial influence on climate
996 (Bond et al., 2013; IPCC, 2013; Liao et al., 2015). It can heat the atmosphere through
997 absorbing solar radiation (Ramanathan and Carmichael, 2008), influence cloud
998 microphysical and dynamical processes (Jacobson, 2006; McFarquhar and Wang,
999 2006), and reduce surface albedo through deposition on snow and ice (Flanner et al.,
1000 2007; Qian et al., 2015).

1001 Due to accelerated urbanization and rapid economic growth, emissions of BC in
1002 China increased dramatically during recent decades. It contributed to about one
1003 fourth of the global emissions of BC in recent decades (Bond et al., 2007). Strong
1004 emissions lead to high concentrations of BC over China. Zhang et al. (2008) collected
1005 aerosol samples at eighteen stations spread over China during 2006 and reported BC
1006 concentrations in a range of 9–14 µg m⁻³ at urban sites, 2–5 µg m⁻³ at rural sites, and
1007 about 0.35 µg m⁻³ at remote background sites. BC also exerts significant positive
1008 direct radiative forcing (DRF) at the top of the atmosphere (TOA) in China. Using the
1009 Regional Climate Chemistry Modeling System (RegCCMs), Zhuang et al. (2013)
1010 reported an annual mean BC DRF of 2–5 W m⁻² at TOA over eastern China and
1011 about 6 W m⁻² over Sichuan Basin in year 2006. Li et al. (2016) also showed a strong
1012 DRF of BC over the North China Plain and Sichuan Basin in most seasons except for
1013 spring when the strongest BC DRF with values of 4–6 W m⁻² shifted to southern
1014 China.

1015 BC is the product of incomplete combustion of fossil fuels, biofuels, and open
1016 burning, such as forest and grassland fires and agricultural waste burning on fields. In
1017 the atmosphere the average lifetime of BC is only a few days, due to both wet
1018 removal and dry deposition, which is much shorter than that of long-lived greenhouse
1019 gases. In addition, BC lifetime is region dependent. BC in East Asia has a shorter
1020 lifetime than the global mean value due to a faster regional removal (H. Wang et al.,

Deleted: 18

1022 2014), probably associated with strong precipitation during monsoon season. BC
1023 emission reductions may benefit both mitigation of global climate change and
1024 regional air quality (Shindell et al., 2012; Bond et al., 2013; Smith and Mizrahi, 2013),
1025 especially in East Asia where fuel combustion emits substantial BC along with other
1026 pollutant species. Many previous observational and/or modeling studies have
1027 examined the source sector contributions of BC over China (Zhuang et al., 2014;
1028 Y.-L. Zhang et al., 2015; Li et al., 2016). They found that residential heating and
1029 industry sectors were the largest contributors to BC concentrations in China, while
1030 biomass burning emissions from outside China were important to BC in western
1031 China. An effective BC reduction in a receptor region would require knowing not only
1032 the source sector that contributes the most to BC levels, but also the source
1033 contributions from various locations within and outside the region. However, very few
1034 previous studies have focused on the source attribution of BC concentrations in
1035 various regions of China. Li et al. (2016) examined the contributions of emissions
1036 inside and outside China to BC over China (with only two source regions) but did not
1037 divide the source contributions from different regions inside China.

1038 Pollution levels also show substantial daily to weekly variation. In recent years,
1039 extreme wintertime hazy conditions occurred frequently in China and caused serious
1040 air pollution, affecting more than half of the 1.3 billion people (Ding and Liu, 2014).
1041 During one winter haze episode in 2013, BC concentrations increased up to about 20
1042 and 8 $\mu\text{g m}^{-3}$ in Xi'an and Beijing over northern China, and 6 and 4 $\mu\text{g m}^{-3}$ in
1043 Guangzhou and Shanghai over southern China, respectively (Y.-L. Zhang et al.,
1044 2015). The transport of pollutants from upwind was reported to be one of the most
1045 important contributors to local high aerosol concentrations during haze days (L. T.
1046 Wang et al., 2014; Y. Yang et al., 2016). L. T. Wang et al. (2014) found that emissions
1047 from northern Hebei and Beijing-Tianjin were the major contributor to particulate
1048 matter ($\text{PM}_{2.5}$) pollution in Shijiazhuang in January 2013. Yang et al. (2016) confirmed
1049 a connection between wind fields and $\text{PM}_{2.5}$ concentrations during winter hazy days
1050 through model simulations and statistical analysis. They also found that weakened
1051 winds contributed to increases in winter aerosol concentrations and hazy days over

1052 eastern China during recent decades. As a chemically inert species, atmospheric BC
1053 is a good tracer to investigate the source region contributions from local and non-local
1054 emissions during polluted conditions that are related to long-range transport.

1055 BC particles originating from East Asia can also be transported across the North
1056 Pacific, reaching North America (Hadley et al., 2007; Ma et al., 2013a; Matsui et al.,
1057 2013; H. Wang et al., 2014; Yang et al., 2015). Matsui et al. (2013) simulated outflow
1058 of BC from East Asia using the Community Multiscale Air Quality (CMAQ) model and
1059 found that anthropogenic emissions from China, biomass burning emissions from
1060 Southeast Asia, and biomass burning emissions from Siberia and Kazakhstan
1061 contributed 61%, 17%, and 6%, respectively, to the eastward BC flux at 150°E
1062 averaged over 2008–2010. Hadley et al. (2007) estimated the trans-Pacific transport
1063 of BC during April of 2004 using the Chemical Weather Forecast System (CFORS)
1064 model and reported that, across 130°W, 75% of BC transported into North America
1065 originated from Asia. Huang et al. (2012) simulated BC using the Sulfur Transport
1066 and Deposition Model (STEM), and found emissions outside North America
1067 contributed to 30–80% of column BC over North America in summer 2008. H. Wang
1068 et al. (2014) examined the long-term (1995–2005) average global source-receptor
1069 relationship of BC and found that BC emitted from the entire East Asia only contribute
1070 less than 5% to the total BC burden in North America, although the contribution is up
1071 to 40% near the west coast region. Few studies have examined the outflow from East
1072 Asia and inflow into North America contributed from source regions in and outside
1073 China. In addition, the emissions of BC from China increased dramatically during the
1074 last few years, with the annual total anthropogenic emissions estimated to have
1075 almost doubled in year 2014 compared to year 2000, shown in the newly developed
1076 Community Emissions Data System (CEDS; Hoesly et al. 2017). Therefore, the
1077 long-range transport of BC and source-receptor relationships could be quite different
1078 from previous studies.

1079 Due to its warming effect in the climate system, BC is potentially important for
1080 climate mitigation and has drawn much attention recently. Source attribution of the
1081 direct radiative effect of BC is likely to be different from that of near-surface

1082 concentration and column burden due to the dependence of radiative forcing on the
1083 vertical distribution of BC and its mixing state with other species that are influenced
1084 by different regional sources. In this study, we use the Community Earth System
1085 Model (CESM) with improved representations of aerosol transport and wet removal (H.
1086 Wang et al., 2013) and a BC source-tagging technique (H. Wang et al., 2014).
1087 Anthropogenic emissions from the newly developed CEDS inventory (Hoesly et al.,
1088 2017), as released for the Coupled Model Intercomparison Project Phase 6 (CMIP6),
1089 are used to examine the source attributions for mass concentration, long-range
1090 transport, and direct radiative forcing of BC in various regions of China. We aim to
1091 quantify: (1) source region contributions to concentrations of BC over various receptor
1092 regions in China; (2) contributions to changes in BC concentrations under polluted
1093 conditions; (3) source contributions to trans-boundary and trans-Pacific transport of
1094 BC; and (4) source contributions to direct radiative forcing of BC in China.

1095 The CESM model, emissions, and numerical experiment are described in
1096 Section 2. Section 3 provides evaluation of the simulated concentration and aerosol
1097 absorption optical depth of BC in China. Section 4 investigates source contributions
1098 to near-surface concentrations, long-range transport and direct radiative forcing of BC
1099 over various receptor regions using the BC source-tagging technique in CESM.
1100 Section 5 summarizes these results.

1101

1102 **2. Methods**

1103 We simulate the evolution and direct radiative forcing (DRF) of BC using CESM
1104 version 1.2 (Hurrell et al., 2013). The atmospheric model in CESM is version 5 of the
1105 Community Atmosphere Model (CAM5), with horizontal grid spacing of 1.9° latitude
1106 by 2.5° longitude and 30 vertical layers ranging from the surface to 3.6 hPa used in
1107 this study. The model treats the properties and processes of major aerosol species
1108 (sea salt, mineral dust, sulfate, black carbon, primary organic matter and secondary
1109 organic aerosol) using a three-mode modal aerosol module (MAM3), in which aerosol
1110 size distributions are represented by three lognormal modes: Aitken, accumulation,
1111 and coarse modes. BC is emitted to the accumulation mode. Mass mixing ratios of

1112 different aerosol species and the number mixing ratio are predicted for each mode. A
1113 more detailed description of the MAM3 representation can be found in Liu et al.
1114 (2012). Aerosol dry deposition velocities are calculated using the Zhang et al. (2001)
1115 parameterization. The wet deposition of aerosols in our CAM5 model includes
1116 in-cloud wet removal (i.e., activation of interstitial aerosols to cloud-borne particles
1117 followed by precipitation scavenging) and below-cloud wet removal (i.e., capture of
1118 interstitial aerosol particles by falling precipitation particles) for both stratiform and
1119 convective clouds. Aerosol activation is calculated with the parameterization of
1120 Abdul-Razzak and Ghan (2000) for stratiform cloud throughout the column and
1121 convective cloud at cloud base, while the secondary activation above convective
1122 cloud base has a simpler treatment with an assumed maximum supersaturation in
1123 convective updrafts (H. Wang et al., 2013). The unified treatment for convective
1124 transport and aerosol wet removal along with the explicit aerosol activation above
1125 convective cloud base was developed by H. Wang et al. (2013) and included in the
1126 CAM5 version being used in this study. This implementation reduces the excessive
1127 BC aloft and better simulates observed BC concentrations in the mid- to
1128 upper-troposphere. Aerosol optical properties for each mode are parameterized
1129 according to Ghan and Zaveri (2007). Refractive indices for aerosols are taken from
1130 the OPAC (optical properties for aerosols and clouds) software package (Koepke and
1131 Schult, 1998), but for BC at solar wavelengths the values are updated from Bond and
1132 Bergstrom (2006). In MAM3, the aging process of BC is neglected by assuming the
1133 immediate mixing of BC with other aerosol species. Direct radiative forcing of BC is
1134 calculated as the difference in the top-of-the-atmosphere net radiative fluxes with and
1135 without BC for the all-sky condition following Ghan (2013).

1136 Anthropogenic emissions used in this study are from the CEDS dataset, as
1137 released for the CMIP6 model experiments (Hoesly et al. 2017). This newly released
1138 emission inventory includes aerosol (black carbon, organic carbon) and aerosol
1139 precursor and reactive compounds (sulfur dioxide, nitrogen oxides, ammonia, carbon
1140 monoxide, and non-methane volatile organic compounds). The emissions are
1141 provided at monthly resolution for each year of 1750–2014 on a 0.5° x 0.5° grid and

1142 include agricultural, energy, industry, residential, international shipping, solvents,
1143 surface transportation, waste treatment, and aircraft sectors. The biomass burning
1144 emissions used in this study are also developed for CMIP6 based on Global Fire
1145 Emission Database (GFED) version 4, Fire Model Intercomparison Project (FireMIP),
1146 visibility-observations and Global Charcoal Database (GCD) data (van Marle et al.
1147 2016).

1148 Figure 1a shows the horizontal spatial distribution of annual emissions of BC
1149 averaged over the most recent 5 years (2010–2014) and the seven geographical
1150 source regions tagged in continental China, including North China (NC), South China
1151 (SC), Southwest China (SW), Central-West China (CW), Northeast China (NE),
1152 Northwest China (NW), and Tibetan Plateau (TP). Figure 1b summarizes the total
1153 seasonal BC emissions in each of these source regions. North China has the largest
1154 annual emissions of BC in China, with maximum emission larger than 1.2 g C m^{-2}
1155 year^{-1} and a regional total emission of $1089 \text{ Gg C year}^{-1}$ (44% of total emissions from
1156 continental China). Annual emissions of BC also have large values over South and
1157 Southwest China, with maximum values in the range of $0.8\text{--}1.2 \text{ g C m}^{-2} \text{ year}^{-1}$,
1158 followed by Central-West and Northeast China. Over the less economically developed
1159 Northwest China and remote region Tibetan Plateau, emissions of BC are much
1160 lower than other regions in China. The seasonal mean emissions of BC also show the
1161 same spatial pattern as the annual means. BC had the largest emissions over North,
1162 South, and Southwest China in all seasons, among which emissions are strongest in
1163 December-January-February (DJF), especially over North China, resulting from
1164 domestic heating. The total seasonal emissions of BC in continental China are 797,
1165 586, 537, and 577 Gg C in DJF, March-April-May (MAM), June-July-August (JJA),
1166 and September-October-November (SON), respectively, which add up to a total
1167 annual BC emissions of 2497 Gg C averaged over years 2010–2014. The
1168 anthropogenic emissions of BC in China in 2010–2014 are larger than those used in
1169 the previous studies for earlier years (Table S1), partly as a result of a higher estimate
1170 of BC emissions from coal coking production. The higher emissions likely lead to
1171 higher concentrations and direct radiative forcing, and source contributions of BC in

Deleted: China

Deleted: China

Deleted: China

Deleted: China

1176 China, compared to the values reported in these studies. The DJF emissions account
1177 for 26–35% of annual total whereas emissions in JJA only account for 17–24% over
1178 the seven source regions in continental China. Total BC emissions from neighboring
1179 regions including rest of East Asia (REA, with China excluded), South Asia (SAS),
1180 Southeast Asia (SEA), and Russia/Belarus/Ukraine (RBU) are shown in Figure 1c.
1181 These source regions outside China are consistent with source regions defined in the
1182 second phase of Hemispheric Transport of Air Pollution (HTAP2). South Asia and
1183 Southeast Asia have relatively high emissions. They may dominate the contribution to
1184 concentrations and direct radiative forcing of BC in China, especially southern and
1185 western China, from foreign sources through long-range transport.

1186 An explicit BC source tagging capability was originally implemented in CAM5 by H.
1187 Wang et al. (2014), through which emissions of BC from independent source regions
1188 and/or sectors can be explicitly tracked. This method quantifies the source–receptor
1189 relationships of BC in any receptor region within a single model simulation without
1190 perturbing emissions from individual source regions or sectors. R. Zhang et al.
1191 (2015a,b) used this method to quantify the source attributions of BC in western North
1192 America, Himalayas, and Tibetan Plateau. The same BC source tagging technique is
1193 implemented to a newer model version (CAM5.3) and applied in this study to quantify
1194 the source attributions of concentration, transport and direct radiative forcing of BC in
1195 various regions of China. BC emissions (anthropogenic plus biomass burning) from
1196 seven geographical source regions, including North China, South China, Southwest
1197 China, Central-West China, Northeast China, Northwest China, Tibetan Plateau in
1198 China, and from rest of the world (RW) are tagged. Transport and physics tendencies
1199 are calculated separately for each tagged BC in the same way as the original BC
1200 simulation in CESM. We choose the seven individual regions (North China, South
1201 China, Southwest China, Central-West China, Northeast China, Northwest China, and
1202 Tibetan Plateau) and all seven regions combined (hereafter continental China) as
1203 receptor regions in this study to examine the source-receptor relationships of BC.
1204 While all emissions, including sulfur dioxides, organic carbon and BC, were used in
1205 the model simulation, tagging was only applied to BC emissions.

1206 The CAM5 simulation is performed at $1.9^\circ \times 2.5^\circ$ horizontal grid spacing using the
1207 specified-dynamics mode (Ma et al., 2013b), in which large-scale circulations (i.e.,
1208 horizontal winds) are nudged to 6-hourly reanalysis data from the Modern Era
1209 Retrospective-Analysis for Research and Applications (MERRA) reanalysis data set
1210 (Rienecker et al., 2011) with a relaxation time scale of 6 hours (K. Zhang et al., 2014).
1211 The use of nudged winds allows for a more accurate simulation so that the key role of
1212 large-scale circulation patterns matches observations over the specified years. The
1213 simulation is run from year 2009 to 2014, with both time-varying aerosol emissions
1214 and meteorological fields. The first year is for spin-up and the last five years are used
1215 for analysis.

1216

1217 3. Model evaluation

1218 The simulations of aerosols, especially BC, using CAM5 have been extensively
1219 evaluated against observations including aerosol mass and number concentrations,
1220 vertical profiles, aerosol optical properties, aerosol deposition, and cloud-nucleating
1221 properties in several previous studies (e.g., Liu et al., 2012, 2016; H. Wang et al.,
1222 2013; Ma et al., 2013b; Jiao et al., 2014; Qian et al., 2014; R. Zhang et al., 2015a,b).
1223 Here we focus on the evaluation of model performance in China using measurements
1224 of near-surface BC concentrations, vertical profiles, aerosol index derived from
1225 satellite, and aerosol absorption optical depth from the Aerosol Robotic Network
1226 (AERONET).

1227 3.1 Mass concentrations and column burden of BC

1228 Figure 2 presents spatial distributions of simulated seasonal mean near-surface
1229 concentrations and column burden of BC, both of which show a similar spatial pattern
1230 to emissions of BC (Figure 1a) with the largest values over North China and the lowest
1231 values over Northwest China and Tibetan Plateau. Near-surface model results are
1232 taken to be the lowest model layer (from surface to 985 hPa in average). Among all
1233 seasons, DJF has the highest BC levels, with values in the range of 6–12, 2–8, and 1–
1234 $8 \mu\text{g m}^{-3}$ for near-surface concentrations and 6–12, 2–8, 1–12 mg m^{-2} for column
1235 burden over North, South, and Southwest China, respectively. In contrast, JJA has

Deleted: many

Deleted: Near-surface m

Deleted: 993

1239 the lowest BC concentrations over China due to the lower emissions and larger wet
1240 scavenging associated with East Asian summer monsoon (Lou et al., 2016).
1241 Averaged over continental China, near-surface BC concentrations are 2.5, 1.1, 0.8,
1242 and 1.4 $\mu\text{g m}^{-3}$ in DJF, MAM, JJA, and SON, respectively, with seasonal variability of
1243 50%. The column burden of BC shows smaller seasonal variability (40%), with
1244 area-weighted average of 2.5, 1.4, 1.0, and 1.4 mg m^{-2} in DJF, MAM, JJA, and SON,
1245 respectively, in China. The magnitude, spatial distribution, and seasonal variations of
1246 simulated near-surface BC concentrations over China are similar to those in Fu et al.
1247 (2012) and X. Wang et al. (2013) using Intercontinental Chemical Transport
1248 Experiment-Phase B (INTEX-B) emission inventory (Zhang et al., 2009) and those in
1249 Li et al. (2016) using HTAP emission inventory (Janssens-Maenhout et al., 2015)
1250 together with a global chemical transport model.

Deleted: It suggests that, besides domestic emissions in China, there are other BC sources from outside China contributing significantly to BC concentrations in the column.

Deleted: Hemispheric Transport of Air Pollution (

Deleted:)

1251 The simulated near-surface BC concentrations are evaluated here using
1252 measurements at fourteen sites of the China Meteorological Administration
1253 Atmosphere Watch Network (CAWNET) (Zhang et al., 2012). The locations of
1254 CAWNET sites are shown in Figure S1a. The observational data include monthly BC
1255 concentrations in years 2006–2007. Note that the simulated BC concentrations are
1256 for years 2010–2014. Figure 3a compares the simulated seasonal mean near-surface
1257 BC concentrations with those from CAWNET observations and Table S2 summarizes
1258 the comparison in different regions, using modeled values from the grid cell
1259 containing each observational site. Simulated BC concentrations at most sites are
1260 within the range of one third to three times of observed values, except for Dunhuang
1261 (94.68°E, 40.15°N) and Lhasa (91.13°E, 29.67°N) sites over western China, where
1262 BC concentrations appear to be underestimated in the model (up to 20 times lower).
1263 The possible bias is discussed in the following part. Over North China, simulated
1264 concentrations are similar to observations in DJF, but underestimated in other
1265 seasons. Over South China, the simulations do not have large biases compared to
1266 the observed BC. However, simulated BC is underestimated in all seasons over
1267 Southwest, Central-West, Northeast, Northwest China, and Tibetan Plateau.
1268 Compared to the CAWNET data, the modeled near-surface BC concentrations have

Deleted: 14

Deleted: 3

1277 a normalized mean bias (NMB) of –48%. Note that anthropogenic BC emissions went
1278 up by a factor of 1.18 between 2006–2007 and 2010–2014. An emissions adjusted
1279 comparison would result in an even larger underestimation. There are several
1280 reasons that might cause low bias in this comparison. Liu et al. (2012) and H. Wang
1281 et al. (2013) have previously found underestimation of BC concentrations over China
1282 in CAM5 model and suggested the BC emissions may be significantly
1283 underestimated. Using the global chemical transport model GEOS-Chem together
1284 with emissions in 2006, Fu et al. (2012) found the simulated BC concentrations in
1285 China were underestimated by 56%. With HTAP emissions at the year 2010 level, Li
1286 et al. (2016) showed a low bias of 37% in simulated BC concentration in China.

1287 Larger wet removal rate and shorter lifetime of aerosols along with the instantaneous
1288 aging of BC in the MAM3 can also lead to the lower concentrations of BC (e.g., Wang
1289 et al., 2011; Liu et al., 2012; H. Wang et al., 2013; Kristiansen et al., 2016).

1290 Another potential cause for a bias in this comparison is spatial sampling bias.
1291 Half of the CAWNET sites are located in urban areas, which will tend to have high
1292 values near sources, whereas the modeled values represent averages over large grid
1293 cells (R. Wang et al., 2014), as further discussed below.

1294 The model captures well the spatial distribution and seasonal variation of BC
1295 concentrations in China, having a statistically significant correlation coefficient of
1296 +0.56 between simulated and observed seasonal BC concentrations over CAWNET
1297 sites.

Deleted: between modeled and

Deleted: values

1298 Figure S2 compares the observed and simulated vertical profiles of BC
1299 concentrations in the East-Asian outflow region. The model successfully reproduces
1300 the vertical profile of BC that was measured in March–April 2009 during the
1301 A-FORCE field campaign and reported by Oshima et al. (2012).

1302 3.2 Aerosol absorption optical depth of BC

1303 To evaluate the simulated aerosol absorption optical depth (AAOD) of BC, the
1304 AAOD data from AERONET (Holben et al., 2001) are used here. The locations of
1305 AERONET sites in China are shown in Figure S1b. The observed AAOD are averaged
1306 over years of 2010–2014 over seven sites and 2005–2010 over three sites with data

Deleted: 7

Deleted: 3

1311 available. Most AERONET sites are over eastern and central China. AAOD of BC at
1312 550nm are calculated by interpolating AAOD at 440 and 675 nm and removing AAOD
1313 of dust from the retrieved AERONET AAOD following Bond et al. (2013). Figure 3b
1314 compares the observed and simulated seasonal mean AAOD of BC at 550nm and
1315 Table S3 summarizes the comparisons in different regions. The model has a low bias
1316 in simulating AAOD of BC in China, smaller than the bias in near-surface
1317 concentrations, with a NMB of -6%. As is the case with surface concentrations, this
1318 bias could be due to model issues, such as BC transport or optical parameterization;
1319 an underestimate in emissions; or spatial sampling bias. Simulated AAOD of BC are
1320 within the range of one third to three times of observed values at most sites, with the
1321 spatial distribution and seasonal variation broadly captured by the model. All but one
1322 of the observations are located in the North and South China regions, and simulated
1323 BC AAOD are, on average, similar to observations there. The AAOD from one
1324 observation site in Central-West China is higher than the modeled value in DJF and
1325 lower in other seasons. Note that, the observed AAOD of BC is derived from
1326 AERONET measurements using the absorption Ångström exponent. A recent study
1327 (Schuster et al., 2016) reported that absorption Ångström exponent is not a robust
1328 parameter for separating out carbonaceous absorption in the AERONET database,
1329 which could cause biases in the AAOD estimates.

Deleted: (Figure 3a)

Deleted: , although spatial sampling bias is likely to be less important for the BC column than for surface concentrations

Deleted: 3

Deleted: Note that a

1330 Figure 4 shows the spatial distribution of simulated seasonal mean AAOD of total
1331 aerosols and Aerosol Index (AI) derived from Ozone Monitoring Instrument (OMI)
1332 measurements over years of 2010–2014. AI is a measure of absorbing aerosols
1333 including BC and dust. Compared to satellite AI data, the model roughly reproduces
1334 spatial distribution of total AAOD in China, with large values over North, South, and
1335 Southwest China in all seasons. AI derived from Total Ozone Mapping Spectrometer
1336 (TOMS) measurements (Figure S3) also shows similar pattern as simulated AAOD. It
1337 should be noted that, besides BC, dust particles also largely contribute to AI and
1338 produces large AI values over Northwest China.

Deleted: some

Deleted: from

Deleted: spatial

Deleted: (Figure S3)

1339 To examine the potential model bias more broadly we compared the difference of
1340 AAOD and AI between western and eastern China (Fig. 4). Averaging AI and AAOD

Deleted: China

1352 broadly over eastern and western China, we find that AAOD/AI is 0.055 over eastern
1353 China and 0.027 over western China. If we assume that the simulated AAOD do not
1354 have large biases over eastern China based on the evaluation against observations
1355 shown above (Fig. 3b and Table S3), then this difference hints a possible
1356 underestimation of BC column burden in the model over the western regions.
1357 However, it is difficult to draw a firm conclusion, given the likely differential role of dust
1358 in eastern vs western China. This differential likely also contributes to AAOD biases in
1359 modeling dust and may also impact biases in the satellite derived AI values.

1360 ▼
1361 **4. Source contributions to BC concentrations, transport and direct radiative**
1362 **forcing**

1363 **4.1. Source contributions to seasonal mean BC concentrations**

1364 Figure 5 shows the simulated spatial distribution of seasonal near-surface BC
1365 concentrations originating from the seven tagged source regions in continental China
1366 and all other sources from outside China (rest of the world, RW) and Table S4
1367 summarizes these source-receptor relationships. It is not surprising that regional
1368 emissions largely influence BC concentrations in the same region. For example,
1369 emissions of BC from North China give $6.3 \mu\text{g m}^{-3}$ of BC concentrations over North
1370 China in DJF, whereas they only account for less than $1.8 \mu\text{g m}^{-3}$ over other regions
1371 in China. However, the relatively small amount of BC from upwind source regions can
1372 also be a large contributor to receptor regions near the strong sources. BC emissions
1373 from North China contribute large amount to concentrations over South, Southwest,
1374 Central-West, and Northeast China. BC emissions from South and Southwest China
1375 also produce a widespread impact on BC over other neighboring regions. The
1376 impacts of BC emitted from the remaining China regions are relatively small both in
1377 local and non-local regions due to weak emissions (Fig. 1b). All the sources in China
1378 have the largest impact in DJF, resulting from the strong BC emissions in winter,
1379 while emissions from outside China have the largest impact on BC over China in
1380 MAM due to the seasonal high emission over Southeast Asia and the strong
1381 springtime southwesterly winds.

Deleted: If we assume the simulated AAOD do not have large bias over eastern China compared to observations, then this difference hints at a possible underestimation of BC column burden in the model over the western regions. It is somewhat difficult to draw a firm conclusion, however, given the likely differential role of dust, and model biases modeling dust, and possible biases in satellite derived AI values. .
Formatted: Indent: First line: 0"

Deleted: biomass burning

1391 Averaged over continental China, emissions of BC from North China produce
1392 mean BC concentrations of 0.4–1.3 $\mu\text{g m}^{-3}$, followed by 0.2–0.5 $\mu\text{g m}^{-3}$ from South
1393 China and 0.1–0.3 $\mu\text{g m}^{-3}$ from Southwest China emissions. For emissions over
1394 Central-West China, Northeast China, Northwest China, and Tibetan Plateau, their
1395 individual impact is less than 0.2 $\mu\text{g m}^{-3}$. In contrast, emissions from outside China
1396 result in 0.12 $\mu\text{g m}^{-3}$ of BC concentrations in China in MAM and less than 0.06 $\mu\text{g m}^{-3}$
1397 in JJA and son. The simulated source contributions to column burden of BC are
1398 shown in Figure S4. They present a very similar spatial distribution and seasonal
1399 variation to those of near-surface BC concentrations. However, the emissions from
1400 outside China have a larger impact on the average column burden of BC over China
1401 than on surface concentrations, with a magnitude of 0.4 mg m^{-2} in MAM, which is
1402 similar to that from sources in North China.

1403 Figure 6 shows the spatial distribution of simulated relative contributions to
1404 near-surface BC concentrations from sources in the seven regions in continental
1405 China and those outside China by season. (The same plots for BC column burden are
1406 shown in Figure S5.) For regions with higher emissions, their BC concentrations are
1407 dominated by local emissions. In contrast, BC levels, especially column burden of BC,
1408 over central and western China with lower emissions are strongly influenced by
1409 non-local sources. Emissions from outside China can be the largest contributor to BC
1410 over these regions. During DJF, MAM and SON, they contribute more than 70% to
1411 both surface concentrations and column burden of BC in Tibetan Plateau, which is
1412 important to the climate change due to the large climate efficacy of BC in snow (Qian
1413 et al., 2011) and acceleration of snowmelt through elevated BC heat pump
1414 mechanism (Lau et al., 2010). BC emissions from outside China also account for a
1415 quite significant fraction of surface concentrations over Northwest and Southwest
1416 China in MAM, which contribute to poor air quality over these regions.

1417 Figure 7 summarizes source attribution for spatially averaged seasonal surface
1418 BC concentrations for the seven receptor regions and continental China combined
1419 (CN). Over North China, the majority of the BC concentrations are attributed to local
1420 emissions in all seasons, with seasonal fractional contributions of 85–94%. Over

1421 South China, the seasonal contributions from local emissions are in the range of 58–
1422 88%. Emissions from North China account for 35% of BC concentrations over South
1423 China in DJF, resulting from the wintertime northwesterly winds (Figure S6a), while
1424 emissions from outside China contribute about 10% in MAM due to the strong
1425 springtime biomass burning over southeast Asia and southwesterly winds transporting
1426 BC from southeast Asia to South China (Figure S6b). Southwest China has a similar
1427 level of local influence, with 47–81% of the BC concentration from local emissions,
1428 whereas 19% are due to emissions from outside China transported by westerly winds
1429 in MAM.

Deleted: world

1430 Non-local emissions from Southwest and North China together contribute 32–44%
1431 of BC concentration in Central-West China. North China emissions play an important
1432 role in BC concentrations over Northeast China, with relative contributions in a range
1433 of 21–30% in MAM, JJA and SON, while only 11% in DJF, which is associated with
1434 northwesterly winds in winter preventing northward transport of BC from North China
1435 to Northeast China. Over Northwest China and Tibetan Plateau, 18–34% and 46–
1436 78%, respectively, of BC originate from emissions outside China due to the low
1437 emissions over the less economically developed western China. For all of continental
1438 China as the receptor, the seasonal BC concentrations are largely attributed to the
1439 emissions from North and South China, with relative contributions ranging from 44–
1440 53% and 18–22%, respectively, followed by contributions from Southwest China (10–
1441 12%) and outside China (5–11%).

Deleted: China

1442 The source region contributions to column burden of BC in each receptor regions
1443 in China are shown in Figure S7. In general, impacts on the non-local BC column
1444 burden are larger than on surface concentrations because aerosol transport is
1445 relatively easier in free-troposphere than in the boundary layer (e.g., Yang et al.,
1446 2015). Column burdens of BC averaged over continental China mainly originate from
1447 emissions in North China, South China and outside China, with relative contributions
1448 ranging from 35–46%, 14–21% and 12–30%, respectively.

Deleted: result

1449
1450 **4.2. Source contributions during polluted days**

1454 Knowing the source attribution of BC during polluted days in China is important for
1455 policy makers, which could provide an effective way for the mitigation of poor air
1456 quality. Here, the polluted days are simply identified as days with daily concentrations
1457 of BC higher than 90th percentile of probability density function in each receptor
1458 regions. A total of different 45 days in winter in the 5-year simulation are identified as
1459 polluted days for each region in China.

1460 Figure 8 shows the DJF composite differences in near-surface BC concentrations
1461 and winds at 850 hPa between polluted and normal days for each receptor region, and
1462 Figure 9 summarizes the local and non-local source contributions to the differences.
1463 When North China is under the polluted condition, BC concentrations are higher by
1464 more than 70% compared to DJF average over North China, with a maximum increase
1465 exceeding $5 \mu\text{g m}^{-3}$. North China local emissions contribute $5.6 \mu\text{g m}^{-3}$ to the
1466 averaged increase in BC concentrations over North China during North China
1467 polluted days, about 90% of the total increase. In winter, eastern China is dominated
1468 by strong northwesterly winds (Figure S6a). The anomalous southerly winds during
1469 polluted days (relative to DJF average) over North China prevent the high BC
1470 concentrations from being transported to South China, leading to a reduced ventilation
1471 and accumulated aerosols in North China.

1472 Over South China, BC concentrations increase by up to $2\text{--}5 \mu\text{g m}^{-3}$, in part due to
1473 the transport from North China by anomalous northerly winds in the north part of
1474 South China in South China polluted days. On average, contribution of North China
1475 emissions to mean concentrations over South China increases by $2.0 \mu\text{g m}^{-3}$ (60% of
1476 total increase) during the South China polluted days.

1477 During polluted days in Southwest China, the anomalous northeasterly winds in
1478 the east part of Southwest China bring in BC from the highly polluted eastern China,
1479 resulting in $2.1 \mu\text{g m}^{-3}$ increase (74% of total increase) in the Southwest China, which
1480 is much larger than the $0.7 \mu\text{g m}^{-3}$ contribution from the Southwest China local
1481 emissions.

1482 The increase in BC concentrations during polluted days over Central-West China
1483 is also largely influenced by the accumulation effect of the anomalous winds over

Deleted: (Fig. 2a)

Deleted: S5a

1486 eastern and central China, which also transport BC from Southwest and eastern China
1487 into the receptor region.

1488 The polluted days in Northeast China are caused by both the accumulation of local
1489 emissions due to the reduced prevailing northeasterly winds and anomalous transport
1490 of BC from North China.

1491 Emissions from outside China could contribute to increases in BC concentrations
1492 over Northwest China and Tibetan Plateau during polluted days. However, during
1493 wintertime regional polluted days in eastern and central China, the contributions of
1494 emissions from outside China do not have a significant influence on the changes in
1495 BC concentrations.

1496 These results suggest that the transport of aerosols plays an important role in
1497 increasing BC concentrations during regional polluted days in eastern and central
1498 China. Reductions in local emissions could benefit mitigation of both local and
1499 non-local haze in China. Emissions from outside China are not as important to hazy
1500 pollution in eastern and central China, where haze episodes occur frequently in winter
1501 due to relatively high anthropogenic aerosol emissions and abnormal meteorological
1502 conditions (Sun et al., 2014; R. H. Zhang et al., 2014; Yang et al., 2016). Note that, in
1503 this study, we only focus on the source-receptor relationships related to the wind
1504 anomalies during polluted days. In addition to winds, changes in other meteorological
1505 fields, such as precipitation, temperature, humidity, and planetary boundary layer
1506 height, could also influence the contributions of local aerosols between polluted and
1507 normal days. Although the BC emissions used in the simulation include a seasonal
1508 variability that could cause some variations in simulated concentrations, the monthly
1509 variability in DJF of BC emissions is less than 4% over China, which is negligible
1510 compared to the differences in concentrations between polluted and normal days.

1511

1512 **4.3. Source contributions to trans-boundary and trans-Pacific transport**

1513 Considering the large contributions of emissions from [South and](#) Southeast Asia
1514 to MAM BC concentrations in the southwest China (Figure 6) and the large outflow of
1515 aerosols from East Asia in springtime (Yu et al., 2008), it is valuable to examine the

1516 inflow and outflow of BC in China. Figures S8a and S8b show the vertical distribution
1517 of source contributions of emissions from outside China to BC concentrations
1518 averaged over 75°–120°E and 25°–35°N, respectively, around the south boundary of
1519 continental China in MAM. High concentrations of BC originating from [South and](#)
1520 Southeast Asia are lifted to the free atmosphere in the south slope of Tibetan Plateau.
1521 Then westerly winds transport these BC particles to Southwest China and South
1522 China in both low- and mid-troposphere. Figures S8c and S8d present the
1523 contributions of emissions from China to BC concentrations averaged over 120°–
1524 135°E and 20°–50°N, respectively, around the east boundary of continental China. In
1525 MAM, the northward meridional winds over 25°–35°N and the southward meridional
1526 winds over 40°–50°N lead to the accumulation of BC in the lower atmosphere in
1527 eastern China. Westerly winds then transport these BC out of China mostly under 500
1528 hPa.

1529 Figure 10 shows the spatial distribution of column burden and surface
1530 concentrations of BC resulting from emissions in and outside China in MAM. Column
1531 burden is used to represent the outflow in this study following previous studies (Chin et
1532 al., 2007; Hadley et al., 2007). There are strong outflows across the Pacific Ocean
1533 originating from emissions both in and outside China. Emissions from China contribute
1534 0.20 mg m^{-2} (or 55%) of MAM mean BC along 150°E averaged over 20°–60°N,
1535 whereas emissions outside China contribute 0.16 mg m^{-2} (or 45%). It suggests that
1536 both emissions from China and outside China are important for the outflow from East
1537 Asia. The yearly contribution from emissions from China [to outflow from East Asia](#) in
1538 this study is 59%, similar to [the contribution of](#) 61% in Matsui et al. (2013) calculated
1539 based on eastward BC mass flux using WRF-CMAQ model with INTEX-B missions.
1540 Averaged over western United States (125°–105°W, 30°–50°N), emissions from
1541 China account for 8% of near-surface BC concentrations and 29% in column burden in
1542 MAM, indicating that emissions from China could have a significant impact on air
1543 quality in western United States. More than half of the China contribution to BC over
1544 western United States originates from eastern China (i.e., the tagged North and South
1545 China).

1546

1547 4.4. Source contributions to direct radiative forcing

1548 The high concentrations of BC in China could also have a significant impact on the
1549 climate system through atmospheric heating or direct radiative forcing. As shown in
1550 Figure 11, the annual mean direct radiative forcing (DRF) of BC at TOA is as high as
1551 3–5 W m⁻² at some locations. Similar to the source attributions of BC concentrations
1552 (Figure 5) and burden (Figure S4), regional sources contribute the largest to DRF over
1553 the respective local regions. Among all the source regions in China, emissions from
1554 North, South, and Southwest China contribute the largest to local DRF of BC, with
1555 maximum DRF in a range of 3–5, 2–3, and 3–5 W m⁻², respectively. Other sources
1556 regions in China have relatively low contributions, with maximum values less than 2 W
1557 m⁻². Emissions outside China lead to 1–2 W m⁻² of DRF of BC over South, Southwest,
1558 Northwest China and Tibetan Plateau, and 0.2–1 W m⁻² over other parts of China, an
1559 effect that is quite widespread.

1560 The total DRF of BC averaged over continental China simulated in this study is
1561 2.20 W m⁻², larger than 0.64–1.55 W m⁻² in previous studies (Wu et al., 2008; Zhuang
1562 et al., 2011; Li et al., 2016), probably due to the different emissions in the time periods
1563 of study, as shown in Table S5. Emissions outside China have the largest
1564 contributions to DRF of BC in China compared to any of the individual source regions
1565 in China, with an averaged contribution of 0.78 W m⁻² (35%). This fractional
1566 contribution from emissions outside China is larger than 25% in Li et al. (2016),
1567 however we use different emissions, model and meteorology. Emissions from North
1568 China result in 0.55 W m⁻² (25%) of DRF of BC over China, followed by 0.30 W m⁻²
1569 (14%) and 0.28 W m⁻² (13%) from Southwest and South China, respectively.
1570 Emissions from Central-West, Northeast, Northwest China, and Tibetan Plateau taken
1571 together account for 0.29 W m⁻² (13%) of DRF of BC over China.

1572 Figure 12a shows the seasonal mean DRF of BC averaged over China as a
1573 function of regional BC emissions. Because of high emissions, DRF of BC emitted
1574 from North China is the largest in all seasons, with values in a range of 0.5–0.8 W m⁻²
1575 averaged over China, followed by 0.2–0.5 W m⁻² from South and Southwest China. BC

Deleted: 75

Deleted: 46

Deleted: Zhuang et al., 2013;

Deleted: The total BC emissions averaged over continental China were 1005 Gg C yr⁻¹ for years 1993–2003 in Wu et al. (2008), 1811 Gg C yr⁻¹ for year 2006 in Zhuang et al. (2011, 2013), and 1840 Gg C yr⁻¹ for year 2010 in Li et al. (2016), whereas 2497 Gg C yr⁻¹ for year 2010–2014 used in this study.

Deleted: China

1586 from the other tagged regions in China contribute less than 0.2 W m^{-2} in all seasons. In
1587 general, BC DRF in each season is proportional to its emission rate.

1588 Figure 12b presents the seasonal DRF efficiency of BC emitted from the tagged
1589 regions and Table S6 summarizes these efficiencies. The variability of DRF efficiency
1590 for forcing over China is determined by several factors, such as incoming solar
1591 radiation (location of source regions), BC column burden and vertical distribution, and
1592 transport out of the region. The China DRF efficiency is largest in western China (NW
1593 and TP). This spatial pattern was also found by Henze et al. (2012). It can be
1594 explained by the increase of multiple scattering effects and attenuation of the
1595 transmitted radiation for large AOD (García et al., 2012). The Northeast China region
1596 has a low China DRF efficiency due to transport eastward outside of China. The
1597 remaining central and southern China regions have China DRF efficiencies that are
1598 fairly consistent, varying by 20-30% about the average. The annual mean and
1599 regional mean DRF efficiency in China is $0.88 \text{ W m}^{-2} \text{ Tg}^{-1}$, within the range of 0.41 –
1600 $1.55 \text{ W m}^{-2} \text{ Tg}^{-1}$ from the previous studies (Table S5).

1601 DRF efficiencies of BC from most regions have higher values in JJA and lower
1602 values in DJF. This is primarily due to more incoming solar radiation in summer.
1603 Insolation is the largest over Northwest China in JJA, together with less precipitation
1604 than other regions, resulting in large DRF efficiency there. Global BC DRF efficiency,
1605 particularly the annual average, is fairly similar for central, southern, and eastern
1606 China regions (Fig. 12c, d). Global efficiency is still much higher for the western
1607 regions.

1608 BC emission reductions may impact mitigation of climate change and improve air
1609 quality. To compare the relative importance of climate and air quality effects of BC
1610 from different regions in China, Fig. 13 shows the near-surface concentration and
1611 column burden efficiency of BC over China and globally and Table S7 summarizes
1612 these efficiencies. For near-surface concentration (Fig. 13a and 13b), the efficiencies
1613 are largest in DJF and lowest in JJA, in contrast to the DRF efficiencies, resulting
1614 from the less precipitation and wet deposition of aerosols in winter. Unlike the DRF
1615 efficiencies, the near-surface concentration efficiencies over eastern China are

1616 similar and even larger than those for central and western China. These results
1617 suggest that reduction in BC emissions in eastern China could benefit more on the
1618 regional air quality in China, especially in winter haze season.

1619 The relative distributions of column burden efficiencies (Fig. 13c and 13d) are
1620 similar to the DRF efficiencies for the major emitting region in China, indicating that
1621 aerosol lifetime in atmosphere drives DRF that influences regional and global climate.
1622 The western regions (NW and TP), as expected, have a higher forcing per unit
1623 column burden.

1624

1625 **5. Conclusions and discussions**

1626 In this study, the Community Earth System Model (CESM) with a source-tagging
1627 technique is used to quantify the contributions of BC emitted from seven regions in
1628 continental China, including North China (NC), South China (SC), Southwest China
1629 (SW), Central-West China (CW), Northeast China (NE), Northwest China (NW), and
1630 Tibetan Plateau (TP), and sources outside China (RW) to concentrations, haze
1631 formation, trans-boundary and trans-Pacific transport, and direct radiative forcing
1632 (DRF) of BC in China. The anthropogenic emissions of BC for years 2010-2014 used
1633 in this study were developed for the Coupled Model Intercomparison Project Phase 6
1634 (CMIP6) from the Community Emissions Data System (CEDS). The annual total
1635 emission of BC from continental China is 2497 Gg C averaged over years 2010–2014.
1636 The model captures well the spatial distribution and seasonal variation in China.
1637 AAOD compares well with measurements, which are largely located in central and
1638 eastern China. Surface BC concentrations are underestimated by 48% compared to
1639 point observations.

1640 The individual source regions are the largest contributors to their local BC
1641 concentration levels. Over North China where the air quality is often poor, about 90%
1642 of near-surface BC concentration is contributed by local emissions. However, some
1643 source regions also impact BC in neighboring regions. Due to the seasonal variability
1644 of winds and emission rates, emissions from North China account for 35% of
1645 near-surface BC concentrations over South China in DJF

1646 (December-January-February), while emissions from outside China contribute about
1647 10% in MAM (March-April-May). Over Southwest China, 19% of BC in MAM comes
1648 from sources outside China. Southwest and North China emissions contribute largely
1649 to BC in Central-West China. North China emissions have a contribution in a range of
1650 21–30% to BC concentrations in Northeast China. Over Northwest China and Tibetan
1651 Plateau, more than 20% and 40% of BC, respectively, originates from emissions
1652 outside China. These indicate that, for regions with high emissions, their BC
1653 concentrations are dominated by local emissions. In contrast, BC levels over central
1654 and western China with lower emissions are more strongly influenced by non-local
1655 emissions. For all continental China as a whole, seasonal BC concentrations are
1656 largely due to emissions from North and South China, with relative contributions
1657 ranging from 44–53% and 18–22%, respectively, followed by contributions from
1658 Southwest (10–12%) and outside China (5–11%).

1659 Emissions from non-local sources together with abnormal winds are one of the
1660 important factors contributing to high winter time pollution events in China. Over
1661 South China, about 60% of the increase in BC concentrations during high pollution
1662 conditions results from North China emissions. The increases in BC concentrations
1663 during polluted days over Southwest, Central-West and Northeast China are strongly
1664 influenced by emissions from eastern China. Emissions from outside China could
1665 contribute significantly to increases in BC concentrations over Northwest China and
1666 Tibetan Plateau during their polluted days. However, emissions from outside China do
1667 not have a significant contribution to haze in eastern and central China, suggesting
1668 that reduction in emissions within China would be needed to mitigate both local and
1669 non-local BC concentrations under high-polluted conditions.

1670 Emissions from regions in and outside China both account for about half of BC
1671 outflow from East Asia, suggesting that emissions from China and other regions are
1672 equally important for the BC outflow from East Asia. Through long-range transport,
1673 emissions from China result in 8% of near-surface BC concentration and 29% in
1674 column burden over western United States in MAM, indicating that emissions from
1675 China could have an impact on air quality in western United States.

Deleted: are

1677 The total DRF of BC averaged over continental China simulated in this study is
1678 2.20 W m^{-2} . Among the tagged regions, emissions outside China have the largest
1679 single contribution to DRF of BC in China, with an average contribution of 35%,
1680 followed by 25%, 14%, and 13% due to emissions from North, South and Southwest
1681 China, respectively. DRF efficiencies over eastern China are small compared to
1682 central and western China in all seasons. For near-surface concentration, the
1683 efficiencies are largest in DJF and lowest in JJA, and efficiencies over eastern China
1684 are similar and even larger than central and western China. These suggest that
1685 reduction in BC emissions over eastern China could benefit more on the regional air
1686 quality in China, especially in winter haze season.

Deleted: It can be explained by the increase of multiple scattering effects and attenuation of the transmitted radiation for large AOD.

1687 Note that the model largely underestimates BC concentrations over China,
1688 compared to the observation, which has also been reported in many previous studies
1689 using different models and different emission inventories (e.g., Liu et al., 2012; Fu et
1690 al., 2012; [Huang et al., 2013](#); H. Wang et al., 2013; [Q. Wang et al., 2014](#); R. Wang et
1691 al., 2014; Li et al., 2016). One possible reason is that in situ measurements are point
1692 observations, while the model does not treat the subgrid variability of aerosols and
1693 assumes aerosols are uniformly distributed over the grid cell. R. Wang et al. (2014)
1694 found a reduction of negative bias (from -88% to -35%) in the modeled surface BC
1695 concentrations when using high-resolution emissions and modeling at $0.5^\circ \times 0.7^\circ$
1696 resolution. This result indicates that the siting of observational stations can result in
1697 an artificial bias when comparing with relatively coarse model results. Further
1698 investigation of this siting/resolution bias is warranted, including investigation on
1699 whether this type of bias might extend, presumably to a lesser extent, also to AAOD
1700 measurements.

Deleted: They find, however, that modeling over the North China Plain at an even higher resolution of 0.1° , further reduced the surface concentration bias there from 29% to 8%.

1701 Further reasons that could contribute to this bias are emission underestimation or
1702 inaccurate aerosol processes in the model. Given that the differences between
1703 modeled and observed AAOD over eastern China are relatively small (-6%), we
1704 conclude that, given current evidence, the total amount of atmospheric BC in these
1705 simulations is reasonable at least in this sub-region.

1713 Over eastern China, the BC concentrations are dominated by local emissions in
1714 this study, with local contribution of 58–94%. The underestimation of simulated BC
1715 concentrations over eastern China is more likely due to either underestimation of
1716 local emissions, too much aerosol removal within these regions, or resolution bias
1717 between observations and model grids. Over western China, 18–78% of the BC
1718 originates from emissions outside China. Thus biases of simulated BC concentrations
1719 could also come from underestimation of emissions outside China and or too much
1720 removal of BC during long-range transport. Satellite data are a promising method to
1721 validate modeling and emissions inventories, given that they do not depend on the
1722 location of observing stations, providing more uniform spatial coverage. A
1723 comparison of modeled AOD and satellite AI provides an indication that the
1724 modeled burden in western China is underestimated, although the role of dust needs
1725 to be better characterized.

1726 Uncertainty in China BC emissions has been estimated as –43% to 93% by Lu et
1727 al. (2011), –50% to 164% by Qin and Xie (2012), ±176% by Kurokawa et al. (2013),
1728 and –28 to 126% by Zhao et al. (2013). The BC emissions estimates used here for
1729 China in 2010 are 40% higher than those of Zhao et al. (2013) and Lu et al. (2011)
1730 and 30% higher than Klimont et al. (2016), in large part due to a higher estimate of
1731 BC emissions from coal coke production. Emissions from coke production are
1732 particularly uncertain given that “there are no measurements for PM_{2.5} and BC
1733 emissions” (Huo et al. 2012) available to guide inventory estimates. Total rest of the
1734 world emissions other than China, which appear to be a major contributor to burdens
1735 over western regions, are within 1% of those from Klimont et al. (2016).

1736 BC aging in the atmosphere is important for BC concentration and its optical
1737 properties, which transforms BC from hydrophobic aggregates to hydrophilic particles
1738 coated with soluble materials. He et al. (2015, 2016a) found that BC optical properties
1739 varied by a factor of two or more due to different coating structures during BC aging
1740 process based on their theoretical and experimental intercomparison. Oshima et al.
1741 (2009) and He et al. (2016b) pointed out that the use of various microphysical BC
1742 aging schemes could significantly improve simulations of BC concentrations,

Deleted: aerosol index (

Deleted:)

Deleted: up to more than

1746 compared to the simplified aging parameterizations. Liu et al. (2012) also reported that
1747 the wet removal rate of BC simulated in standard CAM5 is 60% higher than AeroCom
1748 multi-model mean due to the rapid or instantaneous aging of BC. H. Wang et al. (2013)
1749 showed that the explicit treatment of BC aging process with slow aging assumptions in
1750 CAM5 could significantly increase BC lifetime and the efficiency of BC long-range
1751 transport. In the three-mode aerosol module (MAM3) of CAM5 used in this study, the
1752 aging process of BC is neglected by assuming the immediate internal mixing of BC
1753 with other aerosol species in the same mode. This assumption could lead to an
1754 overestimation of wet removal of BC and, therefore, an underestimation of BC
1755 concentrations, absorption optical depth (Fig. 3) and direct radiative forcing. In
1756 addition, the internally-mixed optical treatment in CAM5 could also cause bias in BC
1757 absorption calculation. However, H. Wang et al. (2014) examined source-receptor
1758 relationships for BC under the different BC aging assumptions and found that the
1759 quantitative source attributions varied slightly while the qualitative source-receptor
1760 relationships still hold. Therefore, although the magnitude of simulated BC and its
1761 optical properties could be underestimated due to the instantaneous aging of BC and
1762 uncertainty in coating structures, we expect that the aging treatment in MAM3 of
1763 CAM5 should not influence the qualitative source attributions examined in this study.

1764 In this study, BC is used as an indicator of pollution (or air quality) in China.
1765 Although BC is often co-emitted with other species, such as primary organic matter,
1766 organic gases and sulfuric gases, source-receptor relationship of BC may not fully
1767 represent that of total aerosols. The contribution of BC to total near-surface PM_{2.5}
1768 concentrations averaged over China is less than 10%. Other aerosols, such as sulfate,
1769 are dominant in China during polluted days. The spatio-temporal variations and
1770 source contributions of these species are largely different from those of BC because
1771 spatial distributions of emissions (e.g., SO₂) and formation processes can be
1772 considerably different. For example, Matsui et al. (2009) showed that primary aerosols
1773 around Beijing were determined by emissions within 100 km around Beijing within the
1774 preceding 24 hours, while emissions as far as 500 km and within the preceding 3 days
1775 were found to affect secondary aerosols in Beijing. Thus, the secondary aerosols

1776 could have larger contributions from non-local emissions than BC. BC concentrations
1777 are highest in winter over China due to higher emissions, while sulfate concentrations
1778 reach maximum in summer when the strong sunlight and high temperature favor the
1779 sulfate formation. Therefore, knowing the accurate source attributions of air pollution
1780 in China requires source tagging for more aerosol species, such as sulfate.

1781

1782 *Acknowledgments.*

1783 This research was supported by the National Atmospheric and Space
1784 Administration's Atmospheric Composition: Modeling and Analysis Program
1785 (ACMAP), award NNH15AZ64I. We also acknowledge additional support from the
1786 U.S. Department of Energy (DOE), Office of Science, Biological and
1787 Environmental Research. The Pacific Northwest National Laboratory is
1788 operated for DOE by Battelle Memorial Institute under contract
1789 DE-AC05-76RLO1830. The CESM project was supported by the National Science
1790 Foundation and the DOE Office of Science. The satellite-derived Total Ozone
1791 Mapping Spectrometer Aerosol Index monthly data sets are obtained from the Web
1792 site at http://disc.sci.gsfc.nasa.gov/data-holdings/PIP/aerosol_index.shtml. The
1793 National Energy Research Scientific Computing Center (NERSC) provided
1794 computational resources. Model results are available through NERSC upon request.

1795 **References**

1796

1797 Abdul-Razzak, H., and Ghan, S. J.: A parameterization of aerosol activation: 2.

1798 Multiple aerosol types, *J. Geophys. Res.*, 105, 6837–6844,

1799 doi:10.1029/1999JD901161, 2000.

1800

1801 Anenberg, S. C., Talgo, K., Arunachalam, S., Dolwick, P., Jang, C., and West, J. J.:

1802 Impacts of global, regional, and sectoral black carbon emission reductions on

1803 surface air quality and human mortality, *Atmos. Chem. Phys.*, 11, 7253-7267,

1804 doi:10.5194/acp-11-7253-2011, 2011.

1805

1806 Bond, T. C., Streets, D. G., Yarber, K. F., Nelson, S. M., Woo, J.-H., and Klimont, Z.:

1807 A technology-based global inventory of black and organic carbon emissions from

1808 combustion, *J. Geophys. Res.*, 109, D14203, doi:10.1029/2003JD003697, 2004.

1809

1810 Bond, T. C., and Bergstrom, R. W.: Light absorption by carbonaceous particles: An

1811 investigative review, *Aerosol. Sci. Technol.*, 40, 27–67,

1812 doi:10.1080/02786820500421521, 2006.

1813

1814 Bond, T. C., Bhardwaj, E., Dong, R., Jogani, R., Jung, S., Roden, C., Streets, D. G.,

1815 and Trautmann, N. M.: Historical emissions of black and organic carbon aerosol

1816 from energy-related combustion, 1850–2000, *Global Biogeochem. Cycles*, 21,

1817 GB2018, doi:10.1029/2006GB002840, 2007.

1818

1819 Bond, T. C., Doherty, S. J., Fahey, D. W., Forster, P. M., Berntsen, T., DeAngelo, B.
1820 J., Flanner, M. G., Ghan, S., Kärcher, B., Koch, D., Kinne, S., Kondo, Y., Quinn,
1821 P. K., Sarofim, M. C., Schultz, M. G., Schulz, M., Venkataraman, C., Zhang, H.,
1822 Zhang, S., Bellouin, N., Guttikunda, S. K., Hopke, P. K., Jacobson, M. Z.,
1823 Kaiser, J. W., Klimont, Z., Lohmann, U., Schwarz, J. P., Shindell, D., Storelvmo,
1824 T., Warren, S. G., and Zender, C. S.: Bounding the role of black carbon in the
1825 climate system: A scientific assessment, *J. Geophys. Res.*, 118, 5380–5552,
1826 doi:10.1002/jgrd.50171, 2013.

1827

1828 Chin, M., Diehl, T., Ginoux, P., and Malm, W.: Intercontinental transport of pollution
1829 and dust aerosols: implications for regional air quality, *Atmos. Chem. Phys.*, 7,
1830 5501-5517, doi:10.5194/acp-7-5501-2007, 2007.

1831

1832 Ding, Y. H., and Liu, Y. J.: Analysis of long-term variations of fog and haze in China in
1833 recent 50 years and their relations with atmospheric humidity, *Sci. China Earth*
1834 *Sci.*, 57, 36–46, doi:10.1007/s11430-013-4792-1, 2014.

1835

1836 Flanner, M. G., Zender, C. S., Randerson, J. T., and Rasch, P. J.: Present day
1837 climate forcing and response from black carbon in snow, *J. Geophys. Res.*, 112,
1838 D11202, doi:10.1029/2006JD008003, 2007.

1839

1840 Fu, T.-M., Cao, J. J., Zhang, X. Y., Lee, S. C., Zhang, Q., Han, Y. M., Qu, W. J., Han,
1841 Z., Zhang, R., Wang, Y. X., Chen, D., and Henze, D. K.: Carbonaceous aerosols
1842 in China: top-down constraints on primary sources and estimation of secondary
1843 contribution, *Atmos. Chem. Phys.*, 12, 2725-2746,
1844 doi:10.5194/acp-12-2725-2012, 2012.

1845

1846 García, O. E., Díaz, J. P., Expósito, F. J., Díaz, A. M., Dubovik, O., Derimian, Y.,
1847 Dubuisson, P., and Roger, J.-C.: Shortwave radiative forcing and efficiency of key
1848 aerosol types using AERONET data, *Atmos. Chem. Phys.*, 12, 5129-5145,
1849 doi:10.5194/acp-12-5129-2012, 2012.

1850

1851 Ghan, S. J., and Zaveri, R. A.: Parameterization of optical properties for hydrated
1852 internally mixed aerosol, *J. Geophys. Res.*, 112, D10201,
1853 doi:10.1029/2006JD007927, 2007.

1854

1855 Ghan, S. J., Technical Note: Estimating aerosol effects on cloud radiative forcing,
1856 *Atmos. Chem. Phys.*, 13, 9971-9974, doi:10.5194/acp-13-9971-2013, 2013.

1857

1858 Hadley, O. L., Ramanathan, V., Carmichael, G. R., Tang, Y., Corrigan, C. E.,
1859 Roberts, G. C., and Mauger, G. S.: Trans-Pacific transport of black carbon and
1860 fine aerosols ($D < 2.5 \mu\text{m}$) into North America, *J. Geophys. Res.*, 112, D05309,
1861 doi:10.1029/2006JD007632, 2007.

1862

1863 He, C., Liou, K.-N., Takano, Y., Zhang, R., Levy Zamora, M., Yang, P., Li, Q., and

1864 Leung, L. R.: Variation of the radiative properties during black carbon aging:

1865 theoretical and experimental intercomparison, *Atmos. Chem. Phys.*, 15,

1866 11967-11980, doi:10.5194/acp-15-11967-2015, 2015.

1867

1868 He, C., Takano, Y., Liou, K.-N., Yang, P., Li, Q., and Mackowski, D. W.:

1869 Intercomparison of the GOS approach, superposition T- matrix method, and

1870 laboratory measurements for black carbon optical properties during aging, *J.*

1871 *Quant. Spectrosc. Ra.*, 184, 287–296, doi:10.1016/j.jqsrt.2016.08.004, 2016a.

1872

1873 He, C., Li, Q., Liou, K.-N., Qi, L., Tao, S., and Schwarz, J. P.: Microphysics-based

1874 black carbon aging in a global CTM: constraints from HIPPO observations and

1875 implications for global black carbon budget, *Atmos. Chem. Phys.*, 16, 3077-3098,

1876 doi:10.5194/acp-16-3077-2016, 2016b.

1877

1878 Henze, D. K., Shindell, D. T., Akhtar, F., R. Spurr, J. D., Pinder, R. W., Loughlin, D.,

1879 Kopacz, M., Singh, K., and Shim, C.: Spatially refined aerosol direct radiative

1880 forcing efficiencies, *Environ. Sci. Technol.*, 46, 9511–9518,

1881 doi:10.1021/es301993s, 2012.

1882

1883 Holben, B. N., Tanré, D., Smirnov, A., Eck, T. F., Slutsker, I., Abuhassan, N.,
1884 Newcomb, W. W., Schafer, J. S., Chatenet, B., Lavenu, F., Kaufman, Y. J.,
1885 Castle, J. V., Setzer, A., Markham, B., Frouin, D. C. R., Halthore, R., Karneli, A.,
1886 O'Neill, N. T., Pietras, C., Pinker, R. T., Voss, K., and Zibordi, G.: An emerging
1887 ground-based aerosol climatology: Aerosol optical depth from AERONET, *J.*
1888 *Geophys. Res.*, 106, 12 067–12 098, 2001.

1889

1890 Huang, Y., Wu, S., Dubey, M. K., and French, N. H. F.: Impact of aging mechanism
1891 on model simulated carbonaceous aerosols, *Atmos. Chem. Phys.*, 13,
1892 6329–6343, doi:10.5194/acp-13-6329-2013, 2013.

1893

1894 Huo, H., Lei, Y., Zhang, Q., Zhao, L. J., and He, K. B.: China's coke industry: Recent
1895 policies, technology shift, and implication for energy and the environment, *Energ.*
1896 *Policy.*, 51, 397–404, doi:10.1016/j.enpol.2012.08.041, 2012.

1897

1898 Hurrell, J. W., Holland, M. M., Gent, P. R., Ghan, S., Kay, J. E., Kushner, P. J.,
1899 Lamarque, J. F., Large, W. G., Lawrence, D., Lindsay, K., Lipscomb, W. H.,
1900 Long, M. C., Mahowald, N., Marsh, D. R., Neale, R. B., Rasch, P., Vavrus, S.,
1901 Vertenstein, M., Bader, D., Collins, W. D., Hack, J. J., Kiehl, J., and Marshall, S.:
1902 The Community Earth System Model A Framework for Collaborative Research,
1903 *B. Am. Meteorol. Soc.*, 94, 1339–1360, 2013.

1904

1905 IPCC, 2013, Climate Change 2013: the Physical Science Basis. Contribution of
1906 Working Group I to the Fifth Assessment Report of the Intergovernmental Panel
1907 on Climate Change. Cambridge University Press, Cambridge, United Kingdom
1908 and New York, NY, USA, p. 1535.

1909

1910 Jacobson, M. Z.: Effects of externally-through-internally-mixed soot inclusions within
1911 clouds and precipitation on global climate, *J. Phys. Chem. A*, 110, 6860–6873,
1912 doi:10.1021/Jp056391r, 2006.

1913

1914 Janssen, N. A. H., Gerlofs-Nijiland, M. E., Lanki, T., Salonen, R. O., Cassee, F.,
1915 Hoek, G., Fischer, P., Brunekreef, B., and Krzyzanowski, M.: Health Effects of
1916 Black Carbon, World Health Organization, Copenhagen, 2012.

1917

1918 Janssens-Maenhout, G., Crippa, M., Guizzardi, D., Dentener, F., Muntean, M.,
1919 Pouliot, G., Keating, T., Zhang, Q., Kurokawa, J., Wankmüller, R., Denier van der
1920 Gon, H., Kuenen, J. J. P., Klimont, Z., Frost, G., Darras, S., Koffi, B., and Li, M.:
1921 HTAP_v2.2: a mosaic of regional and global emission grid maps for 2008 and
1922 2010 to study hemispheric transport of air pollution, *Atmos. Chem. Phys.*, 15,
1923 11411-11432, doi:10.5194/acp-15-11411-2015, 2015.

1924

1925 Jiao, C., Flanner, M. G., Balkanski, Y., Bauer, S. E., Bellouin, N., Berntsen, T. K.,
1926 Bian, H., Carslaw, K. S., Chin, M., De Luca, N., Diehl, T., Ghan, S. J., Iversen, T.,

1927 Kirkevåg, A., Koch, D., Liu, X., Mann, G. W., Penner, J. E., Pitari, G., Schulz, M.,
1928 Seland, Ø., Skeie, R. B., Steenrod, S. D., Stier, P., Takemura, T., Tsigaridis, K.,
1929 van Noije, T., Yun, Y., and Zhang, K.: An AeroCom assessment of black carbon
1930 in Arctic snow and sea ice, *Atmos. Chem. Phys.*, 14, 2399-2417,
1931 doi:10.5194/acp-14-2399-2014, 2014.

1932

1933 Klimont, Z., Kupiainen, K., Heyes, C., Purohit, P., Cofala, J., Rafaj, P.,
1934 Borken-Kleefeld, J., and Schöpp, W.: Global anthropogenic emissions of
1935 particulate matter including black carbon, *Atmos. Chem. Phys. Discuss.*,
1936 doi:10.5194/acp-2016-880, in review, 2016.

1937

1938 Koepke, M. H. P., and Schult, I.: Optical properties of aerosols and clouds: The
1939 software package opac, *Bull. Am. Meteorol. Soc.*, 79, 831–844,
1940 doi:10.1175/1520-0477(1998)079<0831:OPOAAC>2.0.CO;2, 1998.

1941

1942 Kristiansen, N. I., Stohl, A., Oliví, D. J. L., Croft, B., Søvde, O. A., Klein, H.,
1943 Christoudias, T., Kunkel, D., Leadbetter, S. J., Lee, Y. H., Zhang, K., Tsigaridis,
1944 K., Bergman, T., Evangeliou, N., Wang, H., Ma, P.-L., Easter, R. C., Rasch, P. J.,
1945 Liu, X., Pitari, G., Di Genova, G., Zhao, S. Y., Balkanski, Y., Bauer, S. E.,
1946 Faluvegi, G. S., Kokkola, H., Martin, R. V., Pierce, J. R., Schulz, M., Shindell, D.,
1947 Tost, H., and Zhang, H.: Evaluation of observed and modelled aerosol lifetimes

1948 using radioactive tracers of opportunity and an ensemble of 19 global models,
1949 Atmos. Chem. Phys., 16, 3525-3561, doi:10.5194/acp-16-3525-2016, 2016.
1950
1951 Kurokawa, J., Ohara, T., Morikawa, T., Hanayama, S., Janssens-Maenhout, G.,
1952 Fukui, T., Kawashima, K., and Akimoto, H.: Emissions of air pollutants and
1953 greenhouse gases over Asian regions during 2000–2008: Regional Emission
1954 inventory in ASia (REAS) version 2, Atmos. Chem. Phys., 13, 11019-11058,
1955 doi:10.5194/acp-13-11019-2013, 2013.
1956
1957 Lau, K.-M., Kim, M. K., Kim, K.-M., and Lee, W. S.: Enhanced surface warming and
1958 accelerated snow melt in the Himalayas and Tibetan Plateau induced by
1959 absorbing aerosols, Environ. Res. Lett., 5, 025204,
1960 doi:10.1088/1748-9326/5/2/025204, 2010.
1961
1962 Li, K., Liao, H., Mao, Y. H., and Ridley, D. A.: Source sector and region contributions
1963 to concentration and direct radiative forcing of black carbon in China, Atmos.
1964 Environ., 124, 351–366, doi:10.1016/j.atmosenv.2015.06.014, 2016.
1965
1966 Liao, H., Chang, W. Y., and Yang, Y.: Climatic effects of air pollutants over China: A
1967 review, Adv. Atmos. Sci., 32, 115–139, doi:10.1007/s00376-014-0013-x, 2015.
1968

1969 Liu, X., Easter, R. C., Ghan, S. J., Zaveri, R., Rasch, P., Shi, X., Lamarque, J.-F.,
1970 Gettelman, A., Morrison, H., Vitt, F., Conley, A., Park, S., Neale, R., Hannay, C.,
1971 Ekman, A. M. L., Hess, P., Mahowald, N., Collins, W., Iacono, M. J., Bretherton,
1972 C. S., Flanner, M. G., and Mitchell, D.: Toward a minimal representation of
1973 aerosols in climate models: description and evaluation in the Community
1974 Atmosphere Model CAM5, *Geosci. Model Dev.*, 5, 709-739,
1975 doi:10.5194/gmd-5-709-2012, 2012.

1976

1977 Liu, X., Ma, P.-L., Wang, H., Tilmes, S., Singh, B., Easter, R. C., Ghan, S. J., and
1978 Rasch, P. J.: Description and evaluation of a new four-mode version of the Modal
1979 Aerosol Module (MAM4) within version 5.3 of the Community Atmosphere Model,
1980 *Geosci. Model Dev.*, 9, 505-522, doi:10.5194/gmd-9-505-2016, 2016.

1981

1982 Lou, S., Russell, L. M., Yang, Y., Xu, L., Lamjiri, M. A., DeFlorio, M. J., Miller, A. J.,
1983 Ghan, S. J., Liu, Y., and Singh, B.: Impacts of the East Asian Monsoon on
1984 springtime dust concentrations over China, *J. Geophys. Res. Atmos.*, 121, 8137–
1985 8152, doi:10.1002/2016JD024758, 2016.

1986

1987 Lu, Z., Zhang, Q., and Streets, D. G.: Sulfur dioxide and primary carbonaceous
1988 aerosol emissions in China and India, 1996–2010, *Atmos. Chem. Phys.*, 11,
1989 9839-9864, doi:10.5194/acp-11-9839-2011, 2011.

1990

1991 Ma, P.-L., Gattiker, J. R., Liu, X., and Rasch, P. J.: A novel approach for determining
1992 source-receptor relationships in model simulations: a case study of black carbon
1993 transport in northern hemisphere winter, *Environ. Res. Lett.*, 8(2), 024042,
1994 doi:10.1088/1748-9326/8/2/024042, 2013a.
1995
1996 Ma, P.-L., Rasch, P. J., Wang, H., Zhang, K., Easter, R. C., Tilmes, S., Fast, J. D.,
1997 Liu, X., Yoon, J.-H., and Lamarque, J.-F.: The role of circulation features on black
1998 carbon transport into the Arctic in the Community Atmosphere Model version 5
1999 (CAM5), *J. Geophys. Res. Atmos.*, 118, 4657–4669, doi:10.1002/jgrd.50411,
2000 2013b.
2001
2002 Matsui, H., Koike, M., Kondo, Y., Takegawa, N., Kita, K., Miyazaki, Y., Hu, M., Chang,
2003 S.-Y., Blake, D. R., Fast, J. D., Zaveri, R. A., Streets, D. G., Zhang, Q., and Zhu,
2004 T.: Spatial and temporal variations of aerosols around Beijing in summer 2006:
2005 Model evaluation and source apportionment, *J. Geophys. Res.*, 114, D00G13,
2006 doi:10.1029/2008JD010906, 2009.
2007
2008 Matsui, H., Koike, M., Kondo, Y., Oshima, N., Moteki, N., Kanaya, Y., Takami, A., and
2009 Irwin, M.: Seasonal variations of Asian black carbon outflow to the Pacific:
2010 Contribution from anthropogenic sources in China and biomass burning sources
2011 in Siberia and Southeast Asia, *J. Geophys. Res. Atmos.*, 118, 9948–9967,
2012 doi:10.1002/jgrd.50702, 2013.

2013

2014 McFarquhar, G., and Wang, H.: Effects of aerosols on trade wind cumuli over the
2015 Indian Ocean: Model simulations, *Q. J. R. Meteorol. Soc.*, 132, 821–843,
2016 doi:10.1256/qj.04.179, 2006.

2017

2018 Oshima, N., Koike, M., Zhang, Y., Kondo, Y., Moteki, N., Takegawa, N., and
2019 Miyazaki, Y.: Aging of black carbon in outflow from anthropogenic sources using
2020 a mixing state resolved model: Model development and evaluation, *J. Geophys.*
2021 *Res.*, 114, D06210, doi:10.1029/2008JD010680, 2009.

2022

2023 Oshima, N., Kondo, Y., Moteki, N., Takegawa, N., Koike, M., Kita, K., Matsui, H.,
2024 Kajino, M., Nakamura, H., Jung, J. S., and Kim, Y. J.: Wet removal of black
2025 carbon in Asian outflow: Aerosol Radiative Forcing in East Asia (A-FORCE)
2026 aircraft campaign, *J. Geophys. Res.*, 117, D03204, doi:10.1029/2011jd016552,
2027 2012.

2028

2029 Qian, Y., Flanner, M. G., Leung, L. R., and Wang, W.: Sensitivity studies on the
2030 impacts of Tibetan Plateau snowpack pollution on the Asian hydrological cycle
2031 and monsoon climate, *Atmos. Chem. Phys.*, 11, 1929-1948,
2032 doi:10.5194/acp-11-1929-2011, 2011.

2033

2034 Qian, Y., Wang, H., Zhang, R., Flanner, M. G., and Rasch, P. J.: A sensitivity study on
2035 modeling black carbon in snow and its radiative forcing over the Arctic and
2036 Northern China, *Environ. Res. Lett.*, 9, 064001,
2037 doi:10.1088/1748-9326/9/6/064001, 2014.
2038

2039 Qian, Y., Yasunari, T. J., Doherty, S. J., Flanner, M. G., Lau, W. K. M., Ming, J.,
2040 Wang, H., Wang, M., Warren, S. G., and Zhang, R.: Light-absorbing particles in
2041 snow and ice: Measurement and modeling of climatic and hydrological impact,
2042 *Adv. Atmos. Sci.*, 32(1), 64–91, doi:10.1007/s00376-014-0010-0, 2015.
2043

2044 Qin, Y. and Xie, S. D.: Spatial and temporal variation of anthropogenic black carbon
2045 emissions in China for the period 1980–2009, *Atmos. Chem. Phys.*, 12,
2046 4825–4841, doi:10.5194/acp-12-4825-2012, 2012.
2047

2048 Ramanathan, V., and Carmichael, G.: Global and regional climate changes due to
2049 black carbon, *Nat. Geosci.*, 1, 221–227, doi:10.1038/ngeo156, 2008.
2050

2051 Rienecker, M. M., Suarez, M. J., Gelaro, R., Todling, R., Bacmeister, J., Liu, R.,
2052 Bosilovich, M. G., Schubert, S. D., Takacs, L., Kim, G-K, Bloom, S., Chen, J.,
2053 Collins, D., Conaty, A., da Silva, A., Gu, W., Joiner, J., Koster, R. D., Lucchesi,
2054 R., Molod, A., Owens, T., Pawson, S., Pegion, P., Redder, C. R., Reichle, R.,
2055 Robertson, F. R., Ruddick, A. G., Sienkiewicz, M., and Woollen, J.: MERRA:

2056 NASA's Modern-Era Retrospective Analysis for Research and Applications, J.
2057 Climate, 24, 3624–3648, 2011.
2058
2059 Schuster, G. L., Dubovik, O., Arola, A., Eck, T. F., and Holben, B. N.: Remote sensing
2060 of soot carbon – Part 2: Understanding the absorption Ångström exponent,
2061 Atmos. Chem. Phys., 16, 1587-1602, doi:10.5194/acp-16-1587-2016, 2016.
2062
2063 Shindell, D., et al. (2012), Simultaneously mitigating near-term climate change and
2064 improving human health and food security, Science, 335(6065), 183-189,
2065 doi:10.1126/science.1210026.
2066
2067 Shindell, D., Kuylenstierna, J. C. I., Vignati, E., van Dingenen, R., Amann, M.,
2068 Klimont, Z., Anenberg, S. C., Muller, N., Janssens- Maenhout, G., Raes, F.,
2069 Schwartz, J., Faluvegi, G., Pozzoli, L., Kupiainen, K., Höglund-Isaksson, L.,
2070 Emberson, L., Streets, D., Ramanathan, V., Hicks, K., Oanh, N. T. K., Milly, G.,
2071 Williams, M., Demkine, V., and Fowler, D.: Simultaneously Mitigating Near-Term
2072 Climate Change and Improving Human Health and Food Security, Science, 335,
2073 183–189, doi:10.1126/science.1210026, 2012.
2074
2075 Smith, S. J., and Mizrahi, A.: Near-term climate mitigation by short-lived forcings, Proc.
2076 Natl. Acad. Sci, 110(35), 14202-14206, doi:10.1073/pnas.1308470110, 2013.
2077

2078 Sun, Y., Jiang, Q., Wang, Z., Fu, P., Li, J., Yang, T., and Yin, Y.: Investigation of the
2079 sources and evolution processes of severe haze pollution in Beijing in January
2080 2013, *J. Geophys. Res. Atmos.*, 119, 4380–4398, doi:10.1002/2014JD021641,
2081 2014.

2082

2083 Wang, H., Easter, R. C., Rasch, P. J., Wang, M., Liu, X., Ghan, S. J., Qian, Y., Yoon,
2084 J.-H., Ma, P.-L., and Vinoj, V.: Sensitivity of remote aerosol distributions to
2085 representation of cloud–aerosol interactions in a global climate model, *Geosci.*
2086 *Model Dev.*, 6, 765-782, doi:10.5194/gmd-6-765-2013, 2013.

2087

2088 Wang, H., Rasch, P. J., Easter, R. C., Singh, B., Zhang, R., Ma, P.-L., Qian, Y., Ghan,
2089 S. J., and Beagley, N.: Using an explicit emission tagging method in global
2090 modeling of source-receptor relationships for black carbon in the Arctic:
2091 Variations, sources, and transport pathways, *J. Geophys. Res. Atmos.*, 119,
2092 12,888–12,909, doi:10.1002/2014JD022297, 2014.

2093

2094 Wang, L. T., Wei, Z., Yang, J., Zhang, Y., Zhang, F. F., Su, J., Meng, C. C., and
2095 Zhang, Q.: The 2013 severe haze over southern Hebei, China: model evaluation,
2096 source apportionment, and policy implications, *Atmos. Chem. Phys.*, 14,
2097 3151-3173, doi:10.5194/acp-14-3151-2014, 2014.

2098

2099 Wang, M., Ghan, S., Ovchinnikov, M., Liu, X., Easter, R., Kassianov, E., Qian, Y., and
2100 Morrison, H.: Aerosol indirect effects in a multi-scale aerosol-climate model
2101 PNNL-MMF, *Atmos. Chem. Phys.*, 11, 5431-5455,
2102 doi:10.5194/acp-11-5431-2011, 2011.
2103
2104 Wang, Q., Jacob, D. J., Spackman, J. R., Perring, A. E., Schwarz, J. P., Moteki, N.,
2105 Marais, E. A., Ge, C., Wang, J., and Barrett, S. R. H.: Global budget and
2106 radiative forcing of black carbon aerosol: Constraints from pole-to-pole (HIPPO)
2107 observations across the Pacific, *J. Geophys. Res.-Atmos.*, 119, 195–206,
2108 doi:10.1002/2013jd020824, 2014.
2109
2110 Wang, R., Tao, S., Balkanski, Y., Ciais, P., Boucher, O., Liu, J., Piao, S., Shen, H.,
2111 Vuolo, M. R., and Valari, M.: Exposure to ambient black carbon derived from a
2112 unique inventory and high-resolution model, *P. Natl. Acad. Sci. USA*, 111, 2459–
2113 2463, 2014.
2114
2115 Wang, X., Wang, Y., Hao, J., Kondo, Y., Irwin, M., Munger, J. W., and Zhao, Y.:
2116 Top-down estimate of China's black carbon emissions using surface
2117 observations: Sensitivity to observation representativeness and transport model
2118 error, *J. Geophys. Res. Atmos.*, 118, 5781–5795, doi:10.1002/jgrd.50397, 2013.
2119

2120 Wu, J., Fu, C., Xu, Y., Tang, J. P., Wang, W., and Wang, Z.: Simulation of direct
2121 effects of black carbon aerosol on temperature and hydrological cycle in Asia by a
2122 Regional Climate Model, *Meteorol. Atmos. Phys.*, 100(1), 179–193,
2123 doi:10.1007/s00703-008-0302-y, 2008.

2124

2125 Yang, Y., Liao, H., and Lou, S.: Decadal trend and interannual variation of outflow of
2126 aerosols from East Asia: Roles of variations in meteorological parameters and
2127 emissions, *Atmos. Environ.*, 100, 141-153, doi:10.1016/j.atmosenv.2014.11.004,
2128 2015.

2129

2130 Yang, Y., Liao, H., and Lou, S.: Increase in winter haze over eastern China in recent
2131 decades: Roles of variations in meteorological parameters and anthropogenic
2132 emissions, *J. Geophys. Res. Atmos.*, 121, doi:10.1002/2016JD025136, 2016.

2133

2134 Yu, H., Remer, L. A., Chin, M., Bian, H., Kleidman, R. G., and Diehl, T.: A
2135 satellite-based assessment of transpacific transport of pollution aerosol, *J.*
2136 *Geophys. Res.*, 113, D14S12, doi:10.1029/2007JD009349, 2008.

2137

2138 Zhang, K., Wan, H., Liu, X., Ghan, S. J., Kooperman, G. J., Ma, P.-L., Rasch, P. J.,
2139 Neubauer, D., and Lohmann, U.: Technical Note: On the use of nudging for
2140 aerosol–climate model intercomparison studies, *Atmos. Chem. Phys.*, 14,
2141 8631-8645, doi:10.5194/acp-14-8631-2014, 2014.

2142

2143 Zhang, L. M., Gong, S. L., Padro, J., and Barrie, L.: A size-segregated particle dry
2144 deposition scheme for an atmospheric aerosol module, *Atmos. Environ.*, 35,
2145 549-560, doi:10.1016/S1352-2310(00)00326-5, 2001.

2146

2147 Zhang, Q., Streets, D. G., Carmichael, G. R., He, K. B., Huo, H., Kannari, A., Klimont,
2148 Z., Park, I. S., Reddy, S., Fu, J. S., Chen, D., Duan, L., Lei, Y., Wang, L. T., and
2149 Yao, Z. L.: Asian emissions in 2006 for the NASA INTEX-B mission, *Atmos.*
2150 *Chem. Phys.*, 9, 5131-5153, doi:10.5194/acp-9-5131-2009, 2009.

2151

2152 Zhang, R. H., Li, Q., and Zhang, R. N.: Meteorological conditions for the persistent
2153 severe fog and haze event over eastern China in January 2013, *Sci. China Earth*
2154 *Sci.*, 57(1), 26–35, doi:10.1007/s11430-013-4774-3, 2014.

2155

2156 Zhang, R., Wang, H., Hegg, D. A., Qian, Y., Doherty, S. J., Dang, C., Ma, P.-L.,
2157 Rasch, P. J., and Fu, Q.: Quantifying sources of black carbon in western North
2158 America using observationally based analysis and an emission tagging technique
2159 in the Community Atmosphere Model, *Atmos. Chem. Phys.*, 15, 12805-12822,
2160 doi:10.5194/acp-15-12805-2015, 2015a.

2161

2162 Zhang, R., Wang, H., Qian, Y., Rasch, P. J., Easter, R. C., Ma, P.-L., Singh, B.,
2163 Huang, J., and Fu, Q.: Quantifying sources, transport, deposition, and radiative

2164 forcing of black carbon over the Himalayas and Tibetan Plateau, *Atmos. Chem.*
2165 *Phys.*, 15, 6205-6223, doi:10.5194/acp-15-6205-2015, 2015b.

2166

2167 Zhang, X. Y., Wang, Y. Q., Zhang, X. C., Guo, W., and Gong, S. L.: Carbonaceous
2168 aerosol composition over various regions of China during 2006, *J. Geophys.*
2169 *Res.*, 113, D14111, doi:10.1029/2007JD009525, 2008.

2170

2171 Zhang, X. Y., Wang, Y. Q., Niu, T., Zhang, X. C., Gong, S. L., Zhang, Y. M., and Sun,
2172 J. Y.: Atmospheric aerosol compositions in China: spatial/temporal variability,
2173 chemical signature, regional haze distribution and comparisons with global
2174 aerosols, *Atmos. Chem. Phys.*, 12, 779-799, doi:10.5194/acp-12-779-2012,
2175 2012.

2176

2177 Zhang, Y.-L., Huang, R.-J., El Haddad, I., Ho, K.-F., Cao, J.-J., Han, Y., Zotter, P.,
2178 Bozzetti, C., Daellenbach, K. R., Canonaco, F., Slowik, J. G., Salazar, G.,
2179 Schwikowski, M., Schnelle-Kreis, J., Abbaszade, G., Zimmermann, R.,
2180 Baltensperger, U., Prévôt, A. S. H., and Szidat, S.: Fossil vs. non-fossil sources of
2181 fine carbonaceous aerosols in four Chinese cities during the extreme winter haze
2182 episode of 2013, *Atmos. Chem. Phys.*, 15, 1299-1312,
2183 doi:10.5194/acp-15-1299-2015, 2015.

2184

2185 Zhao, Y., Zhang, J., and Nielsen, C. P.: The effects of recent control policies on
2186 trends in emissions of anthropogenic atmospheric pollutants and CO₂ in China,
2187 Atmos. Chem. Phys., 13, 487-508, doi:10.5194/acp-13-487-2013, 2013.
2188

2189 Zhuang, B. L., Jiang, F., Wang, T. J., Li, S., and Zhu, B.: Investigation on the direct
2190 radiative effect of fossil fuel black-carbon aerosol over China, Theor. Appl.
2191 Climatol., 104(3), 301–312, doi:10.1007/s00704-010-0341-4, 2011.
2192

2193 Zhuang, B. L., Liu, Q., Wang, T. J., Yin, C. Q., Li, S., Xie, M., Jiang, F., and Mao, H.
2194 T.: Investigation on semi-direct and indirect climate effects of fossil fuel black
2195 carbon aerosol over China, Theor. Appl. Climatol., 114 (3), 651–672,
2196 doi:10.1007/s00704-013-0862-8, 2013.
2197

2198 Zhuang, B. L., Wang, T. J., Liu, J., Li, S., Xie, M., Yang, X. Q., Fu, C. B., Sun, J. N.,
2199 Yin, C. Q., Liao, J. B., Zhu, J. L., and Zhang, Y.: Continuous measurement of
2200 black carbon aerosol in urban Nanjing of Yangtze River Delta, China, Atmos.
2201 Environ., 89, 415–424, doi:10.1016/j.atmosenv.2014.02.052, 2014.
2202
2203
2204
2205

2206 **Figure Captions**

2207

2208 **Figure 1.** (a) Spatial distribution of annual mean total emissions (anthropogenic plus
2209 biomass burning, units: $\text{g C m}^{-2} \text{ yr}^{-1}$) of black carbon (BC) averaged over 2010–2014.
2210 The geographical BC source regions are selected as North China (NC, 109°E–east
2211 boundary, 30°–41°N), South China (SC, 109°E–east boundary, south boundary–
2212 30°N), Southwest China (SW, 100°–109°N, south boundary–32°N), Central-West
2213 China (CW, 100°–109°N, 32°N–north boundary), Northeast China (NE, 109°E–east
2214 boundary, 41°N–north boundary), Northwest China (NW, west boundary–100°E,
2215 36°N–north boundary), and Tibetan Plateau (TP, west boundary–100°E, south
2216 boundary–36°N) in China and regions outside of China (RW, rest of the world). (b)
2217 Seasonal mean total emissions (units: Gg C , $\text{Gg} = 10^9\text{g}$) of BC from the seven BC
2218 source regions in China and emissions from rest of East Asia (REA, with China
2219 excluded), South Asia (SAS), Southeast Asia (SEA), and Russia/Belarus/Ukraine
2220 (RBU).

2221

2222 **Figure 2.** Simulated seasonal mean near-surface concentrations (left, units: $\mu\text{g m}^{-3}$)
2223 and column burden (right, units: mg m^{-2}) of BC in December-January-February (DJF),
2224 March-April-May (MAM), June-July-August (JJA), and
2225 September-October-November (SON).

2226

2227 **Figure 3.** Comparisons of observed and modeled seasonal mean (a) near-surface
2228 concentrations (units: $\mu\text{g m}^{-3}$) and (b) aerosol absorption optical depth (AAOD) of BC
2229 in China. Solid lines mark the 1:1 ratios and dashed lines mark the 1:3 and 3:1 ratios.
2230 Observed BC concentrations were taken between 2006 and 2007 at 14 sites of the
2231 China Meteorological Administration (CMA) Atmosphere Watch Network (CAWNET)
2232 (Zhang et al., 2012). Observed AAOD of BC are obtained by removing dust AAOD
2233 from total AAOD at 10 sites of the Aerosol Robotic Network (AERONET) (Holben et
2234 al., 2001), following Bond et al. (2013). The observed AAOD are averaged over years
2235 of 2005–2014 with data available. Correlation coefficient (R) and normalized mean

2236 bias (NMB) between observation and simulation are shown on top left of each panel.
2237 $NMB = 100\% \times \sum(M_i - O_i) / \sum O_i$, where M_i and O_i are the modeled and observed
2238 values at site i , respectively. Site locations are shown in Figure S1a.

2239

2240 **Figure 4.** Spatial distribution of seasonal mean AAOD of total aerosols (left) and
2241 Aerosol Index (AI) derived from Ozone Monitoring Instrument (OMI) measurements
2242 over years of 2010–2014 (right).

2243

2244 **Figure 5.** Spatial distribution of seasonal mean near-surface concentrations of BC
2245 ($\mu\text{g m}^{-3}$) originating from the seven source regions in China (NC, SC, SW, CW, NE,
2246 NW, and TP), marked with black outlines, and sources outside China (RW).
2247 Regionally averaged BC in China contributed by individual source regions is shown at
2248 the bottom right of each panel.

2249

2250 **Figure 6.** Spatial distribution of relative contributions (%) to seasonal mean
2251 near-surface BC concentrations from each of the tagged source regions.

2252

2253 **Figure 7.** Relative contributions (%) from the tagged source regions (denoted by
2254 colors) to regional mean surface concentrations of BC over seven receptor regions in
2255 China (NC, SC, SW, CW, NE, NW, and TP) and China (seven regions combined, CN)
2256 in different seasons. The receptor regions are marked on the horizontal axis in each
2257 panel.

2258

2259 **Figure 8.** Composite differences in winds at 850 hPa (m s^{-1}) and near-surface BC
2260 concentrations ($\mu\text{g m}^{-3}$) between polluted and normal days in DJF.

2261

2262 **Figure 9.** Composite differences in surface BC concentrations ($\mu\text{g m}^{-3}$) averaged
2263 over receptor regions (marked on the horizontal axis) over eastern and central China
2264 between polluted and normal days in DJF originating from individual sources regions
2265 (bars in each column).

2266

2267 **Figure 10.** Spatial distribution of (a, b) column burden (mg m^{-2}) and (c, d)
2268 near-surface concentrations ($\mu\text{g m}^{-3}$) of BC originating from total emissions inside
2269 (CN) and outside China (RW), respectively, in March-April-May (MAM). The black
2270 solid lines over western (150°E , $20^\circ\text{--}60^\circ\text{N}$) Pacific in panel (a) mark the
2271 cross-sections used to quantify outflow of BC from East Asia. The box over western
2272 United States ($125^\circ\text{--}105^\circ\text{W}$, $30^\circ\text{--}50^\circ\text{N}$) in panel (c) is used to quantify BC
2273 concentrations attributed to sources from China.

2274

2275 **Figure 11.** Spatial distribution of annual mean direct radiative forcing of BC (W m^{-2}) at
2276 the top of the atmosphere originating from the tagged BC source regions in China
2277 (NC, SC, SW, CW, NE, NW, and TP) and source outside China (RW). Regionally
2278 averaged forcing in China contributed by individual source regions is shown at the
2279 bottom right of each panel.

2280

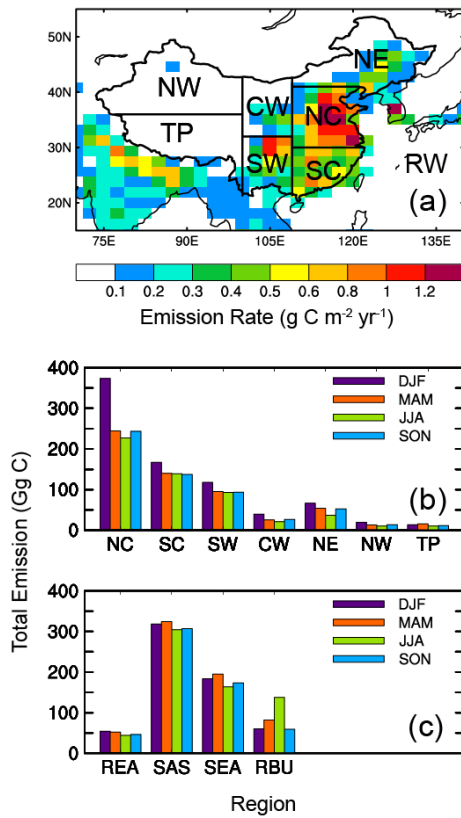
2281 **Figure 12.** (a, c) BC seasonal DRF averaged over China as a function of BC
2282 emission fraction (the ratio of regional emission to the total emission over China and
2283 global, respectively, unit: %) for each of the tagged regions. (b, d) Seasonal DRF
2284 efficiency of BC ($\text{W m}^{-2} \text{Tg}^{-1}$) for each of the tagged source regions over China and
2285 globally, respectively. The efficiency is defined as the DRF divided by the
2286 corresponding scaled annual emission (seasonal emission multiplied by 4). Error bars
2287 indicate $1\text{-}\sigma$ of mean values during years 2010–2014.

2288

2289 **Figure 13.** Seasonal (a, b) near-surface concentration ($\mu\text{g m}^{-3} \text{Tg}^{-1}$) and (c, d) column
2290 burden ($\text{mg m}^{-2} \text{Tg}^{-1}$) efficiency of BC for each of the tagged source regions over
2291 China and globally, respectively.

2292

2293

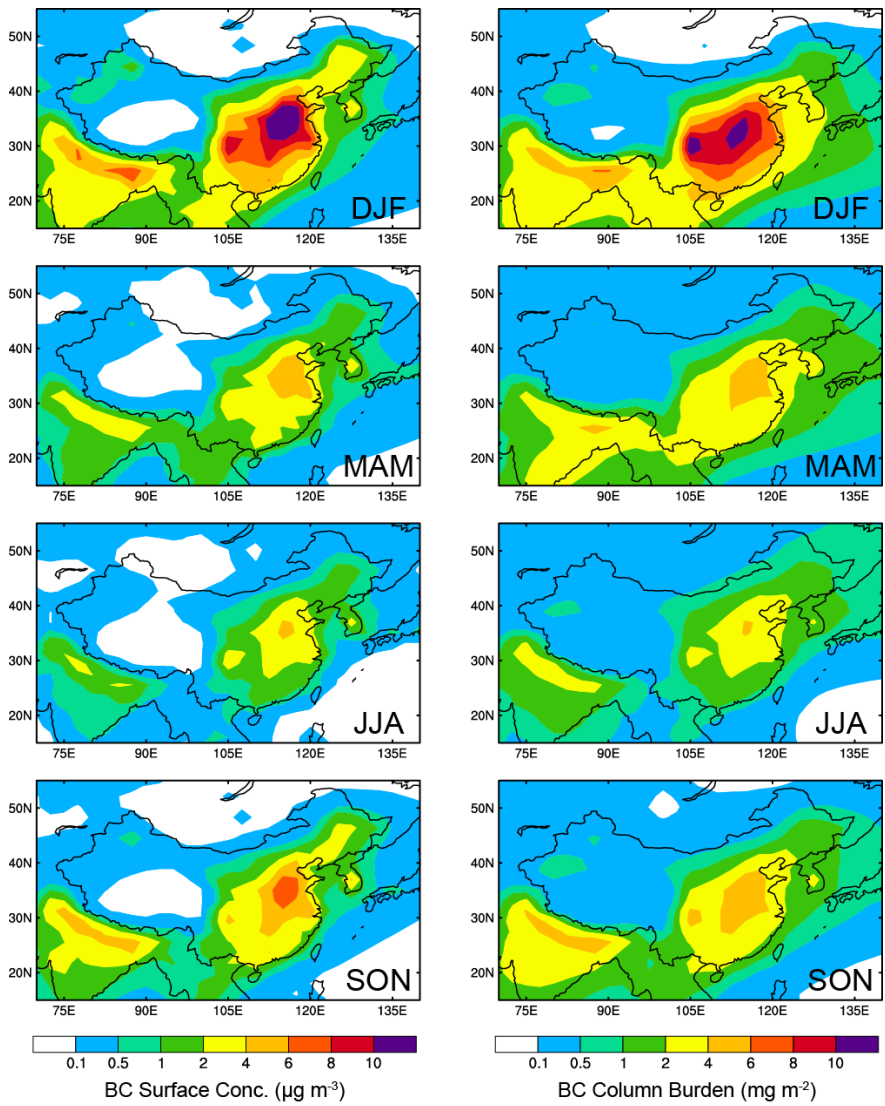


2294

2295

2296 **Figure 1.** (a) Spatial distribution of annual mean total emissions (anthropogenic plus
 2297 biomass burning, units: $\text{g C m}^{-2} \text{ yr}^{-1}$) of black carbon (BC) averaged over 2010–2014.
 2298 The geographical BC source regions are selected as North China (NC, 109°E–east
 2299 boundary, 30°–41°N), South China (SC, 109°E–east boundary, south boundary–
 2300 30°N), Southwest China (SW, 100°–109°E, south boundary–32°N), Central-West
 2301 China (CW, 100°–109°E, 32°N–north boundary), Northeast China (NE, 109°E–east
 2302 boundary, 41°N–north boundary), Northwest China (NW, west boundary–100°E,
 2303 36°N–north boundary), and Tibetan Plateau (TP, west boundary–100°E, south
 2304 boundary–36°N) in China and regions outside of China (RW, rest of the world). (b)
 2305 Seasonal mean total emissions (units: Gg C , $\text{Gg} = 10^9\text{g}$) of BC from the seven BC

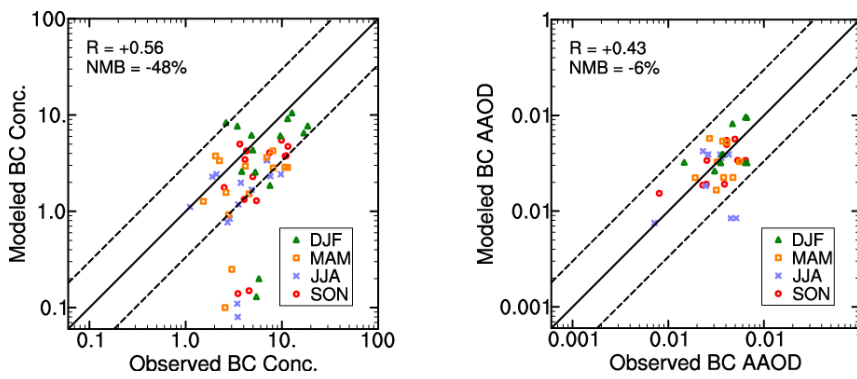
2306 source regions in China and (c) emissions from rest of East Asia (REA, with China
2307 excluded), South Asia (SAS), Southeast Asia (SEA), and Russia/Belarusia/Ukraine
2308 (RBU).



2309

2310

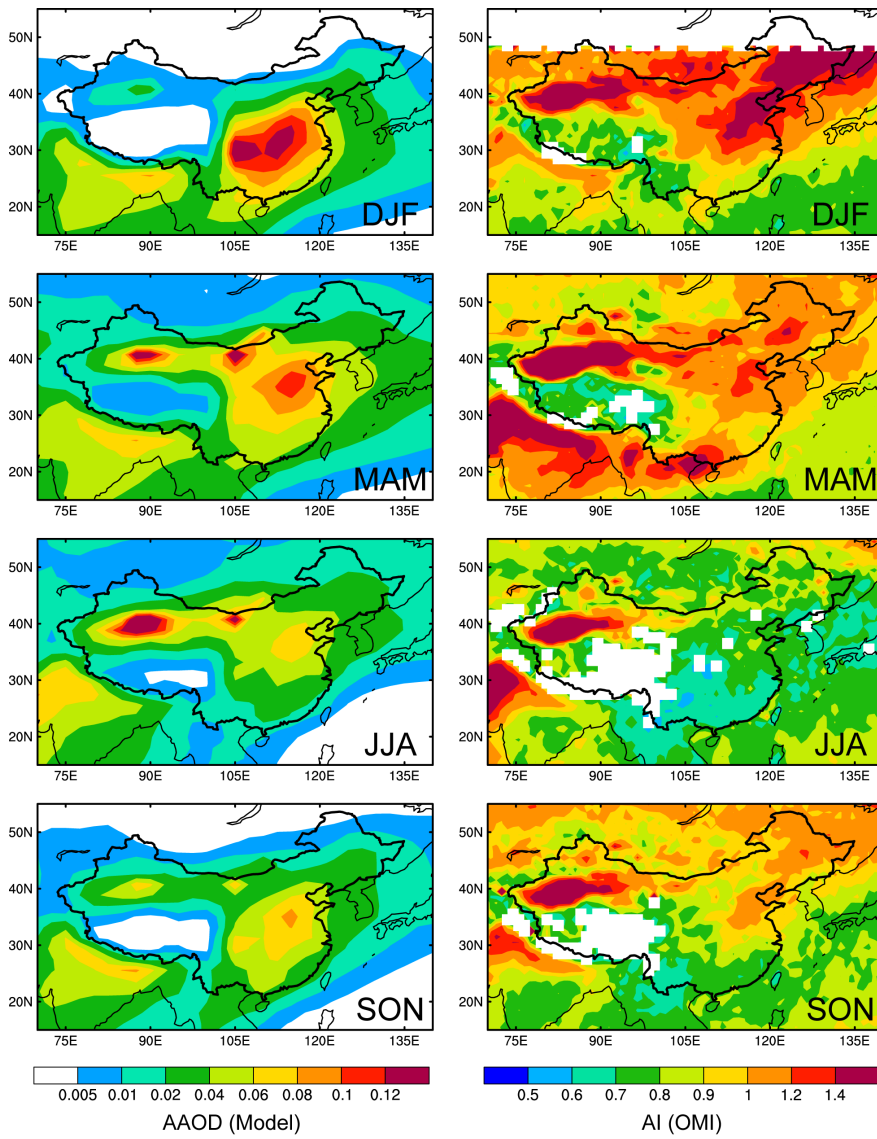
2311 **Figure 2.** Simulated seasonal mean near-surface concentrations (left, units: $\mu\text{g m}^{-3}$)
 2312 and column burden (right, units: mg m^{-2}) of BC in December-January-February (DJF),
 2313 March-April-May (MAM), June-July-August (JJA), and
 2314 September-October-November (SON).



2315
2316

2317 **Figure 3.** Comparisons of observed and modeled seasonal mean (a) near-surface
 2318 concentrations (units: $\mu\text{g m}^{-3}$) and (b) aerosol absorption optical depth (AAOD) of BC
 2319 in China. Solid lines mark the 1:1 ratios and dashed lines mark the 1:3 and 3:1 ratios.
 2320 Observed BC concentrations were taken between 2006 and 2007 at 14 sites of the
 2321 China Meteorological Administration (CMA) Atmosphere Watch Network (CAWNET)
 2322 (Zhang et al., 2012). Observed AAOD of BC are obtained by removing dust AAOD
 2323 from total AAOD at 10 sites of the Aerosol Robotic Network (AERONET) (Holben et
 2324 al., 2001), following Bond et al. (2013). The observed AAOD are averaged over years
 2325 of 2010–2014 over 7 sites and 2005–2010 over 3 sites with data available.
 2326 Correlation coefficient (R) and normalized mean bias (NMB) between observation
 2327 and simulation are shown on top left of each panel. $\text{NMB} = 100\% \times \sum(M_i - O_i) / \sum O_i$,
 2328 where M_i and O_i are the modeled and observed values at site i , respectively. Site
 2329 locations are shown in Figure S1a.

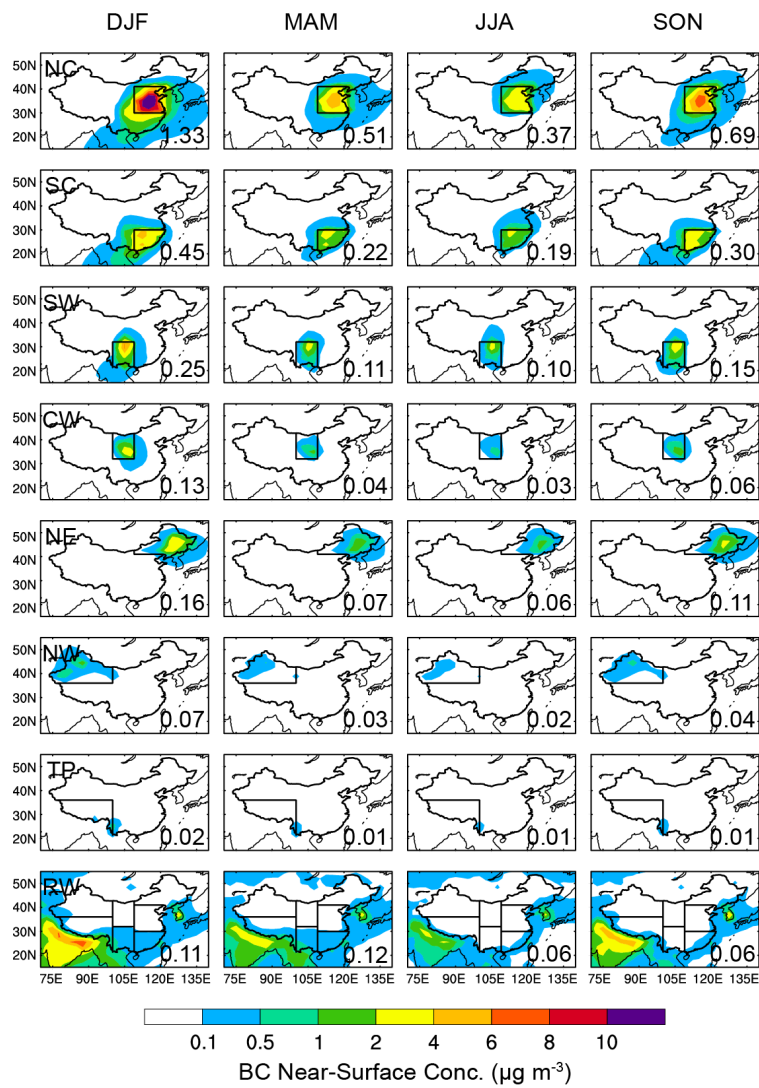
2330
2331



2332

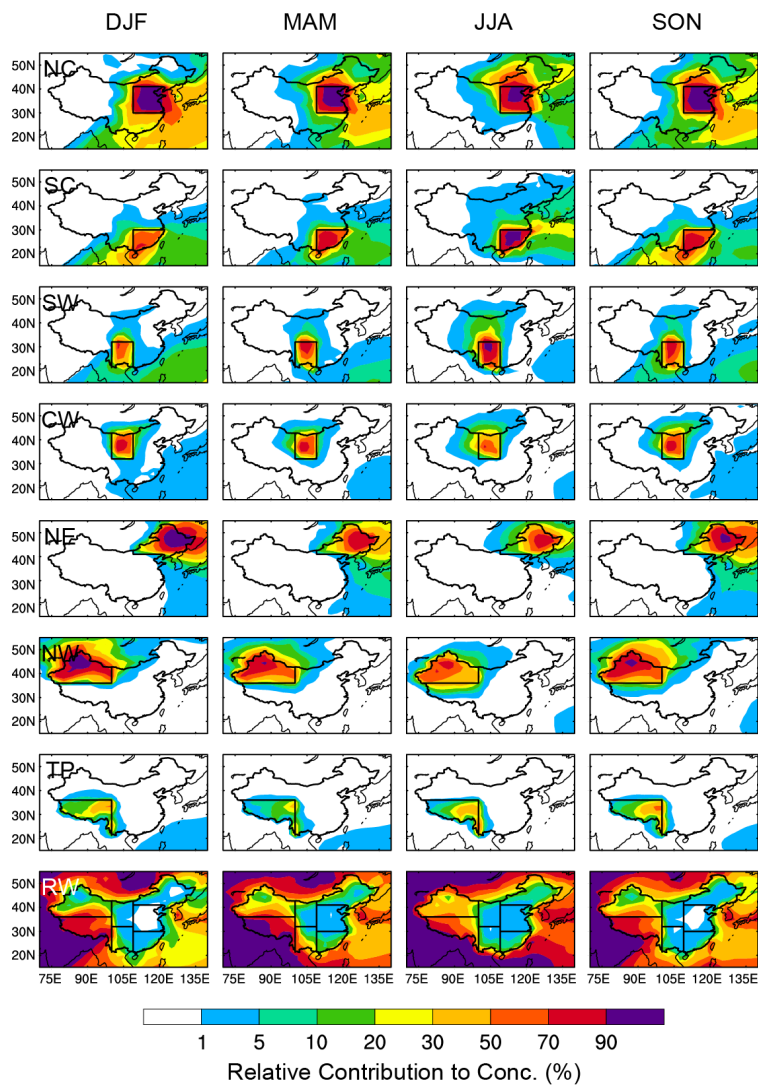
2333

2334 **Figure 4.** Spatial distribution of seasonal mean AAOD of total aerosols (left) and
 2335 Aerosol Index (AI) derived from Ozone Monitoring Instrument (OMI) measurements
 2336 over years of 2010–2014 (right).



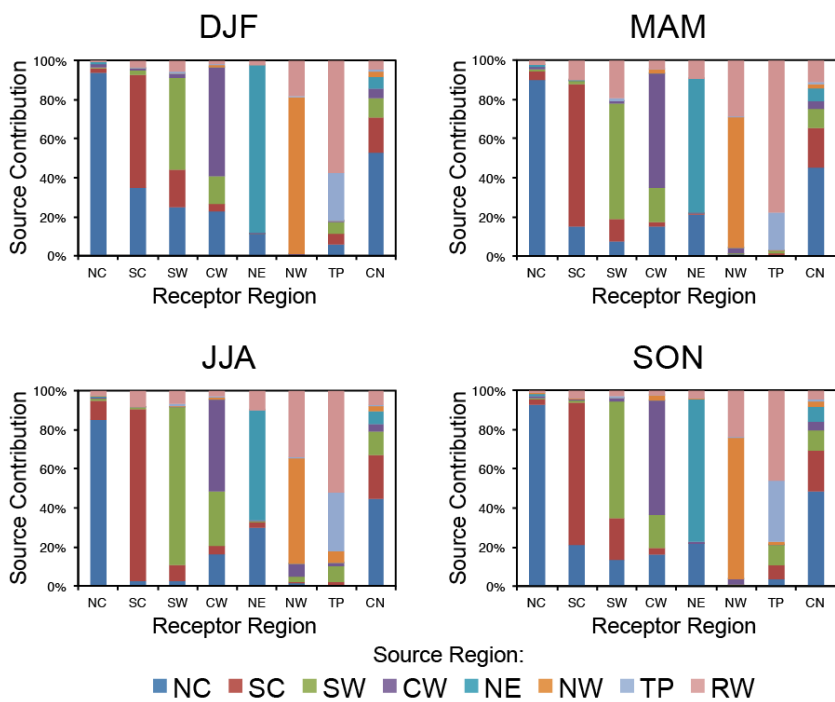
2337
2338

2339 **Figure 5.** Spatial distribution of seasonal mean near-surface concentrations of BC
 2340 ($\mu\text{g m}^{-3}$) originating from the seven source regions in China (NC, SC, SW, CW, NE,
 2341 NW, and TP), marked with black outlines, and sources outside China (RW).
 2342 Regionally averaged BC in China contributed by individual source regions is shown at
 2343 the bottom right of each panel.



2344
 2345
 2346
 2347
 2348

Figure 6. Spatial distribution of relative contributions (%) to seasonal mean near-surface BC concentrations from each of the tagged source regions.



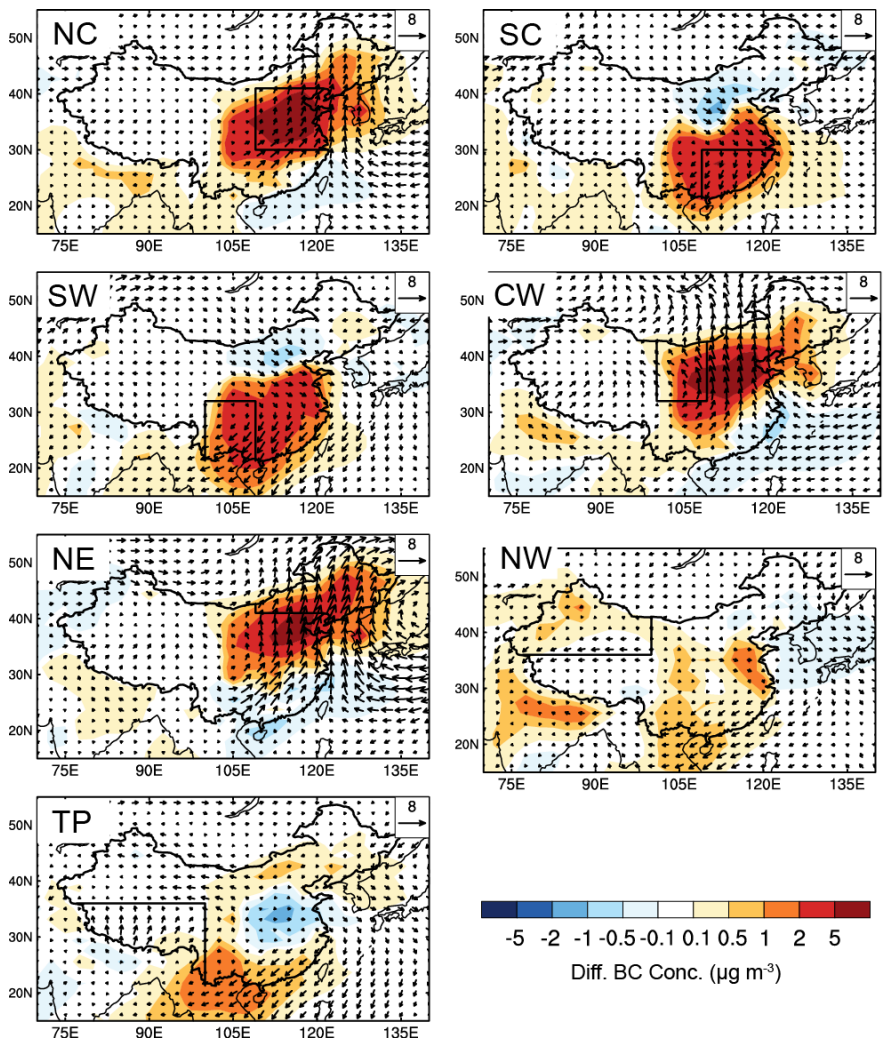
2349

2350

2351 **Figure 7.** Relative contributions (%) from the tagged source regions (denoted by
 2352 colors) to regional mean surface concentrations of BC over seven receptor regions in
 2353 China (NC, SC, SW, CW, NE, NW, and TP) and China (seven regions combined, CN)
 2354 in different seasons. The receptor regions are marked on the horizontal axis in each
 2355 panel.

2356

2357

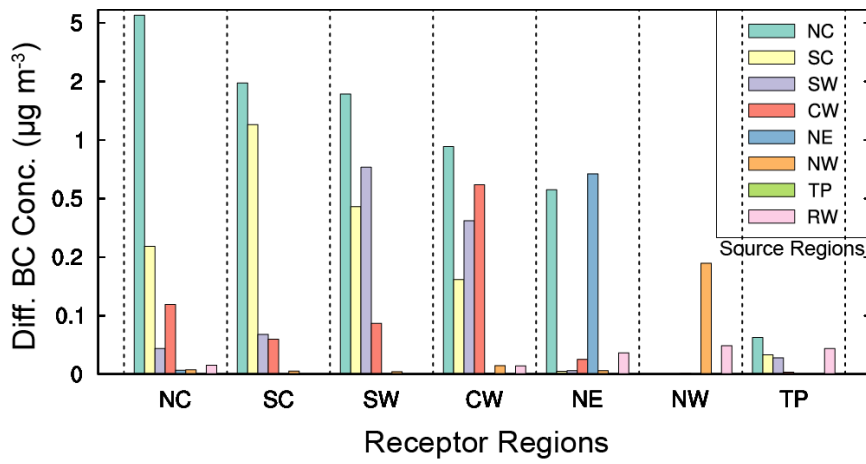


2358

2359

2360 **Figure 8.** Composite differences in winds at 850 hPa (m s^{-1}) and near-surface BC
 2361 concentrations ($\mu\text{g m}^{-3}$) between polluted and normal days in DJF.

2362

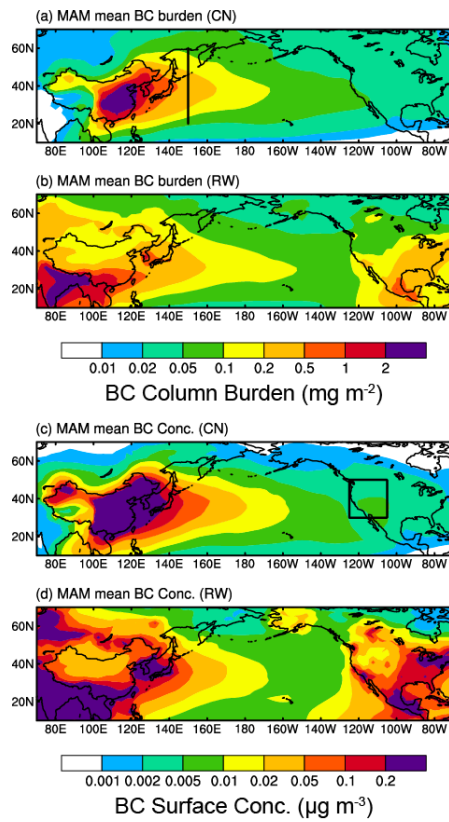


2363

2364

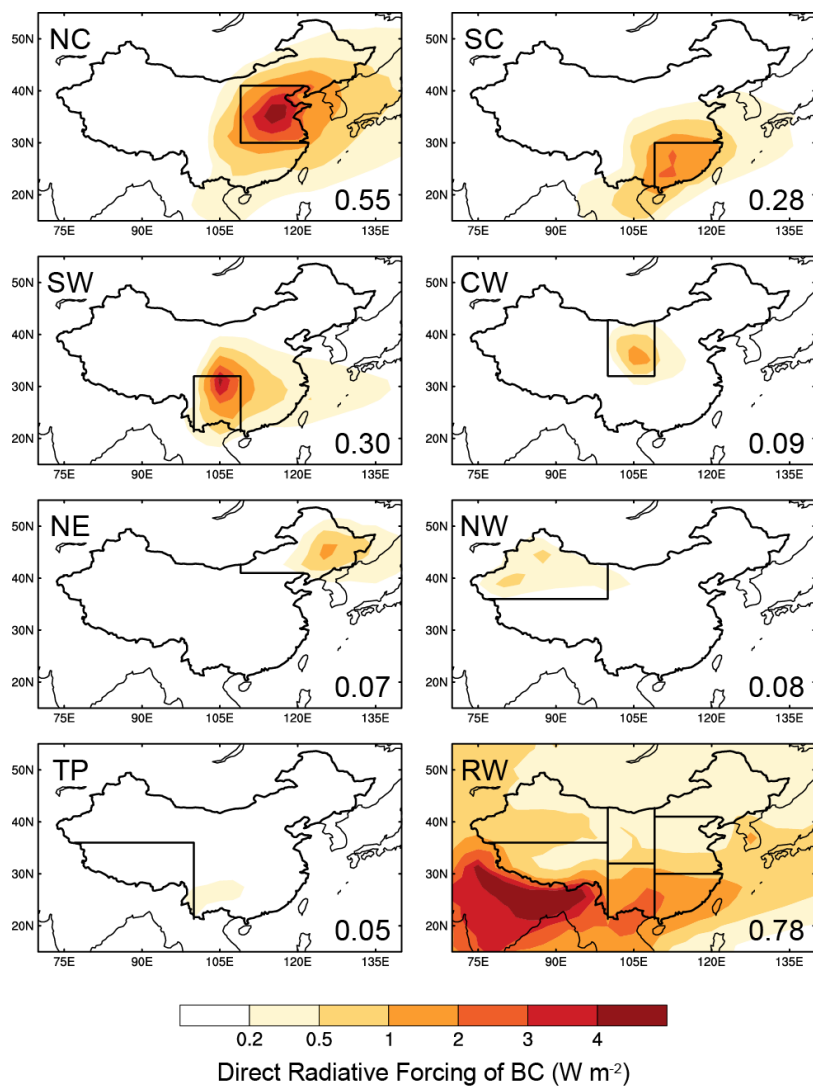
2365 **Figure 9.** Composite differences in surface BC concentrations ($\mu\text{g m}^{-3}$) averaged
 2366 over receptor regions (marked on the horizontal axis) over eastern and central China
 2367 between polluted and normal days in DJF originating from individual sources regions
 2368 (bars in each column).

2369



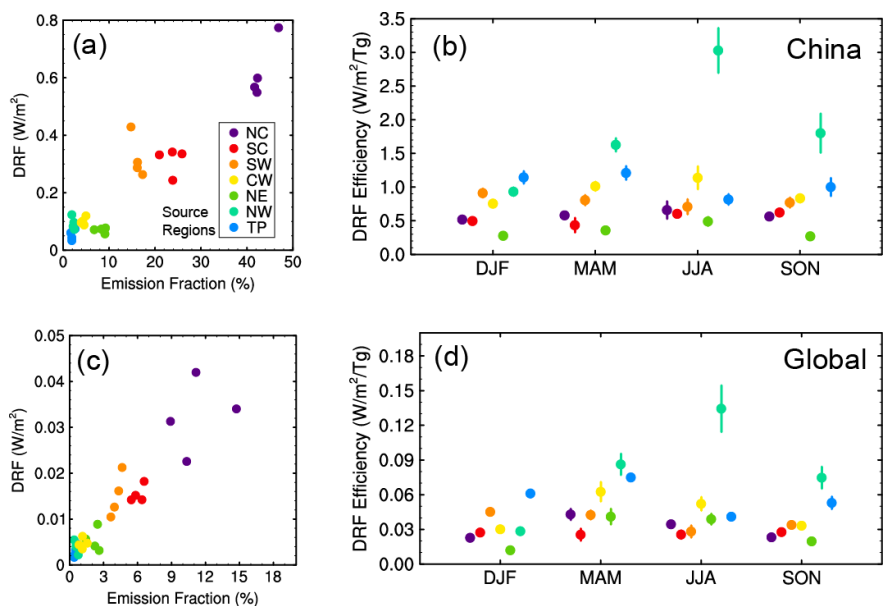
2370
2371

2372 **Figure 10.** Spatial distribution of (a, b) column burden (mg m^{-2}) and (c, d)
 2373 near-surface concentrations ($\mu\text{g m}^{-3}$) of BC originating from total emissions inside
 2374 (CN) and outside China (RW), respectively, in March-April-May (MAM). The black
 2375 solid lines over western (150°E , 20° – 60°N) Pacific in panel (a) mark the
 2376 cross-sections used to quantify outflow of BC from East Asia. The box over western
 2377 United States (125° – 105°W , 30° – 50°N) in panel (c) is used to quantify BC
 2378 concentrations attributed to sources from China.



2379
2380

2381 **Figure 11.** Spatial distribution of annual mean direct radiative forcing (DRF) of BC (W
2382 m^{-2}) at the top of the atmosphere originating from the tagged BC source regions in
2383 China (NC, SC, SW, CW, NE, NW, and TP) and source outside China (RW).
2384 Regionally averaged forcing in China contributed by individual source regions is
2385 shown at the bottom right of each panel.



2386

2387

2388

2389

2390

2391

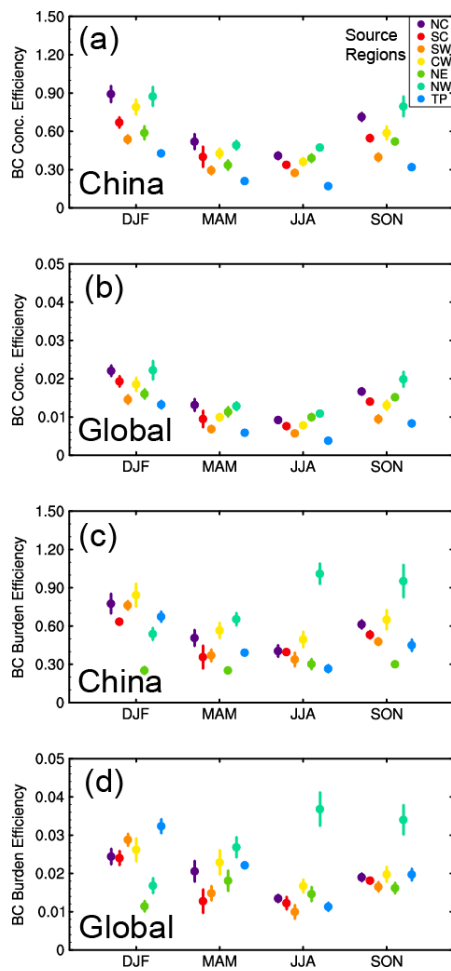
2392

2393

2394

2395

Figure 12. (a, c) BC seasonal DRF averaged over China as a function of BC emission fraction (the ratio of regional emission to the total emission over China and global, respectively, unit: %) for each of the tagged regions. (b, d) Seasonal DRF efficiency of BC ($W m^{-2} Tg^{-1}$) for each of the tagged source regions over China and globally, respectively. The efficiency is defined as the DRF divided by the corresponding scaled annual emission (seasonal emission multiplied by 4). Error bars indicate 1- σ of mean values during years 2010–2014.



2396
 2397
 2398
 2399
 2400
 2401

Figure 13. Seasonal (a, b) near-surface concentration ($\mu\text{g m}^{-3} \text{Tg}^{-1}$) and (c, d) column burden ($\text{mg m}^{-2} \text{Tg}^{-1}$) efficiency of BC for each of the tagged source regions over China and globally, respectively.